The Iranian Journal of Mechanical Engineering Transactions of ISME
Journal homepage: https://jmee.isme.ir/
Vol. 26, No. 1, 2025, pp. 6-30

Research Paper

DOI: https://doi.org/10.30506/jmee.2024.2024337.1343

Thermoelasticity of Functionally Graded Cylindrical Shells under Axisymmetric Partial Thermal Shock

Mehdi Karimi[*]
M.Sc. Student

Mohammad Reza Eslami[†]
Professor

In this paper, we investigate the coupled thermoelastic behavior of a cylindrical shell made of functionally graded material subjected to axisymmetric partial heat shock, employing the theory of classical coupled thermoelasticity. The thermal and mechanical properties of the cylindrical FGM shell, graded through its thickness, are assumed to follow a power-law distribution for the metal and ceramic constituents. We consider the second-order shear deformation shell theory, which accounts for transverse shear strains and rotations. The equations of motion are derived from Hamilton's principle, coupled with the heat conduction equation. These resulting equations are simultaneously solved using the Galerkin finite element method in the spatial domain and Newmark's numerical method in the temporal domain. Finally, we present the temperature and stress distribution along the shell length over time. The results indicate that an increase in the power-law index, leading to an increase in the ceramic volume proportion, results in a higher vibration frequency and a lower vibration magnitude. These results are validated using known data from the literature.

Keywords: Coupled thermoelasticity, Cylindrical shell, Functionally graded materials, Partial shock

1 Introduction

Rapid heating of engineering structures is a common occurrence in industrial applications, and from a scientific standpoint, it can lead to several critical conditions. One of the most significant among these is the propagation of stress front waves or heat-induced vibrations within these structures.

---

[*] M.Sc. Student, Department of Mechanical Engineering, Amirkabir University of Technology, Tehran, Iran, mksz@aut.ac.ir.

[†] Corresponding author, Professor, Department of Mechanical Engineering, Amirkabir University of Technology, Tehran, Iran, eslami@aut.ac.ir

Received: 2024/05/15, Revised: 2024/08/09, Accepted: 2024/09/01

When the duration of the thermal shock load is significantly shorter than the period of the structure's lowest natural frequency, it is recommended to conduct stress analysis using coupled thermoelasticity [1].

Numerous research efforts have been dedicated to the analysis of coupled thermoelastic behavior in structural members:

McQuillen and Brull [2] presented an analytical solution for the dynamic thermoelastic response of homogeneous cylindrical shells, both of finite and infinite lengths. Their findings emphasized the greater importance of dynamic analysis over static analysis in thermal shock situations, particularly as the shell thickness decreases. They also discussed the use of semi-coupled and complete coupled thermoelasticity analysis.

Eslami et al. [3] explored the behavior of thin, homogeneous cylindrical shells under thermal and mechanical shocks. They tackled this problem in the spatial and temporal domains using the Galerkin and Newmark methods, respectively, considering the equations of motion and energy as coupled phenomena.

Sherief and Hamza [4] delved into the realm of coupled thermoelasticity in thick plates. They subjected these plates to symmetrical axial thermal and mechanical shock loads, solving the equations of motion and energy concurrently through the Laplace method and Fourier expansion.

Reddy and Chin [5] applied thermal shock to cylindrical and plate geometries constructed from functionally graded material. They utilized the finite element method to investigate dynamic thermoelastic responses, comparing results between coupled and non-coupled equations while accounting for temperature-dependent properties.

Eslami et al. [6] employed the Galerkin finite element method to analyze shells of revolution, utilizing the Lord-Shulman coupled thermoelasticity model to explore the impact of normal stress and coupling.

Shiari and Eslami [7] considered a composite cylindrical shell subjected to thermal and mechanical shock loads. They adopted the Flugee second-order shell theory, incorporating normal stress, and employed the finite element method with Galerkin and Newmark techniques to compare results between coupled and uncoupled modes.

Bagri and Eslami [8] presented a one-dimensional generalized thermoelasticity model for a disk based on the Lord–Shulman theory. They solved this problem in spatial and temporal domains using the Laplace and Galerkin techniques, respectively, examining the dynamic thermoelastic response under axisymmetric thermal shock loads and the effects of relaxation time and coupling coefficient.

Bakhshi et al. [9] studied the coupled thermoelastic response of a functionally graded annular disk based on the classical theory of thermoelasticity.

Bahtui and Eslami [10] investigated the response of a circular cylindrical thin shell made of functionally graded material based on the generalized theory of thermoelasticity, examining the effects of temperature field distributions across the shell thickness.

Babaei et al. [11] explored the finite element solution of an Euler–Bernoulli beam constructed from functionally graded material subjected to lateral thermal shock loads, considering the effect of the coupling coefficient.

Bagri and Eslami [12] considered the generalized coupled thermoelasticity based on the Lord–Shulman model, including the second sound effect, to analyze the dynamic thermoelastic response of a functionally graded annular disk. They employed the Laplace method to remove time variation from equations, followed by solving them in the spatial domain using the Galerkin method and obtaining answers in the time domain through numerical inverse Laplace transformation, with a focus on relaxation time and coupling coefficient.

Hosseini [13] presented a coupled thermoelasticity analysis of a finite functionally graded hollow cylinder using the Green–Naghdi theory without energy dissipation, obtaining time histories of radial displacement, temperature, and stress distribution for various power-law exponents.

Heydarpour and Aghdam [14] used the generalized coupled thermoelasticity based on the Lord–Shulman theory to study the transient thermoelastic behavior of a rotating functionally graded truncated conical shell subjected to thermal shock under different boundary conditions. They analyzed governing equations using the mapping differential quadrature method and the Newmark technique.

Jafarinezhad and Eslami [15] focused on studying an annular plate made of functionally graded materials under the coupled theory of thermoelasticity, exploring the effects of power-law index, coupling coefficient, and different geometric proportions.

Esmaeili et al. [16] investigated large amplitude thermally induced vibrations in cylindrical shells made of functionally graded material (FGM), assuming thermo-mechanical properties of the FGM shell vary with temperature and thickness coordinates.

Zeverdejani and Kiani [17] examined the coupled and nonlinear thermo-mechanical response of a functionally graded material (FGM) hollow sphere under thermal shock, utilizing the GDQ method, Newmark time marching scheme, and Picard successive algorithm to solve governing equations and obtain temperature, displacement, and stress profiles as functions of time.

Sakha and Eslami [18] analyzed the generalized thermoelastic response of a beam subjected to partial lateral thermal shock, using the Galerkin finite element method and the time marching algorithm to solve the one-dimensional dynamic problem, incorporating quadratic shape functions for the temperature field and C^1-continuous shape functions for the displacement field.

In our study, we investigate the thermoelastic response of a cylindrical shell under symmetrical axial local heat shock. The shell is constructed from functionally graded material and follows Hooke's law. We assume small displacements under applied loads, allowing us to use linear strain-displacement relationships. To derive the complete set of equations governing the shell's behavior, we employ Hamilton's principle, considering both the equations of motion and the coupled heat conduction equation. These equations are solved in the spatial and temporal domains using the Galerkin finite element method and the Newmark technique, respectively. Our results encompass varying values of the coupling coefficient and volume ratios of materials within the FGM. Additionally, we explore the necessity of employing coupled thermoelasticity in cases of rapid thermal loading speeds.

2 Analysis

We consider an FGM cylindrical shell with a radius of R, thickness of h, and length of L, as depicted in Figure (1).

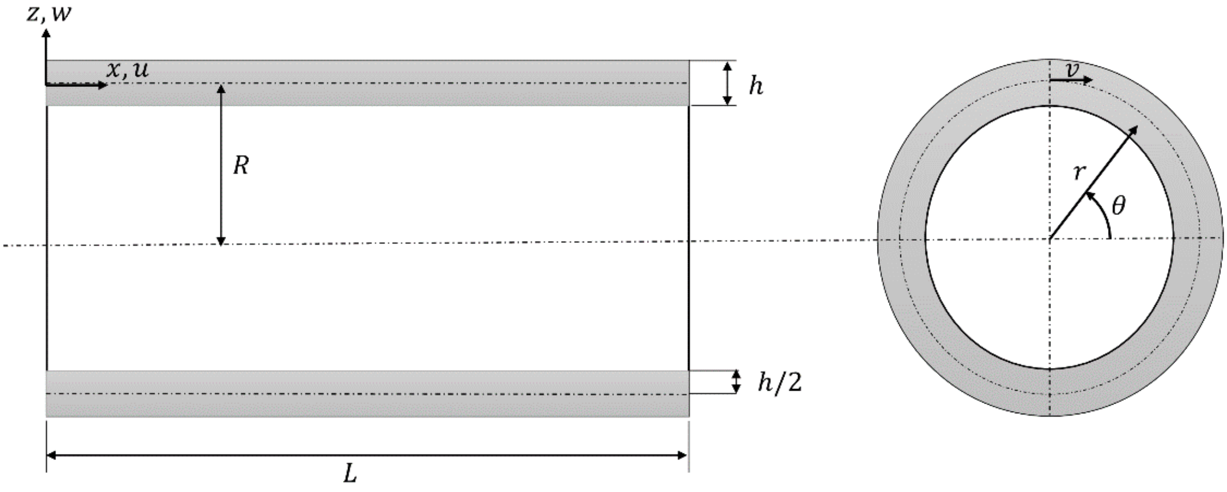

Figure 1 Cylindrical shell whit displacement field.

This functionally graded shell is composed of both metal and ceramic materials, with their properties continuously varying in the thickness direction as a function of the coordinate z, where z represents the shell thickness coordinate ranging from $-h/2$ to $h/2$ with positive values extending outward.

The material properties, including Young's modulus $E(z)$, coefficient of thermal expansion $\alpha(z)$, coefficient of heat conduction $K(z)$, specific heat $C(z)$, and mass density $\rho(z)$, are defined across the shell's thickness. The volume fractions of the constituent materials are denoted as follows:

$$f_m = \frac{V_m}{V_m+V_c} \qquad f_c = \frac{V_c}{V_m+V_c} \tag{1}$$

Here, f_m and f_c represent the volume fractions of the metal and ceramic components in the FGM, respectively, and they satisfy the following equation:

Equation (2) expresses the relationship between the volume fractions of the metal (f_m) and ceramic (f_c) components in the FGM, satisfying the constraint:

$$f_m + f_c = 1 \tag{2}$$

The effective material properties of functionally graded materials can be described as:

$$F_{cf}(z) = F_m f_m + F_c f_c \tag{3}$$

Here, F_m and F_c represent the inherent material properties of each phase.

The volume fraction is assumed to follow a power-law function:

$$f_m = \left(\frac{2z+h}{2h}\right)^i \qquad f_c = 1 - f_m \tag{4}$$

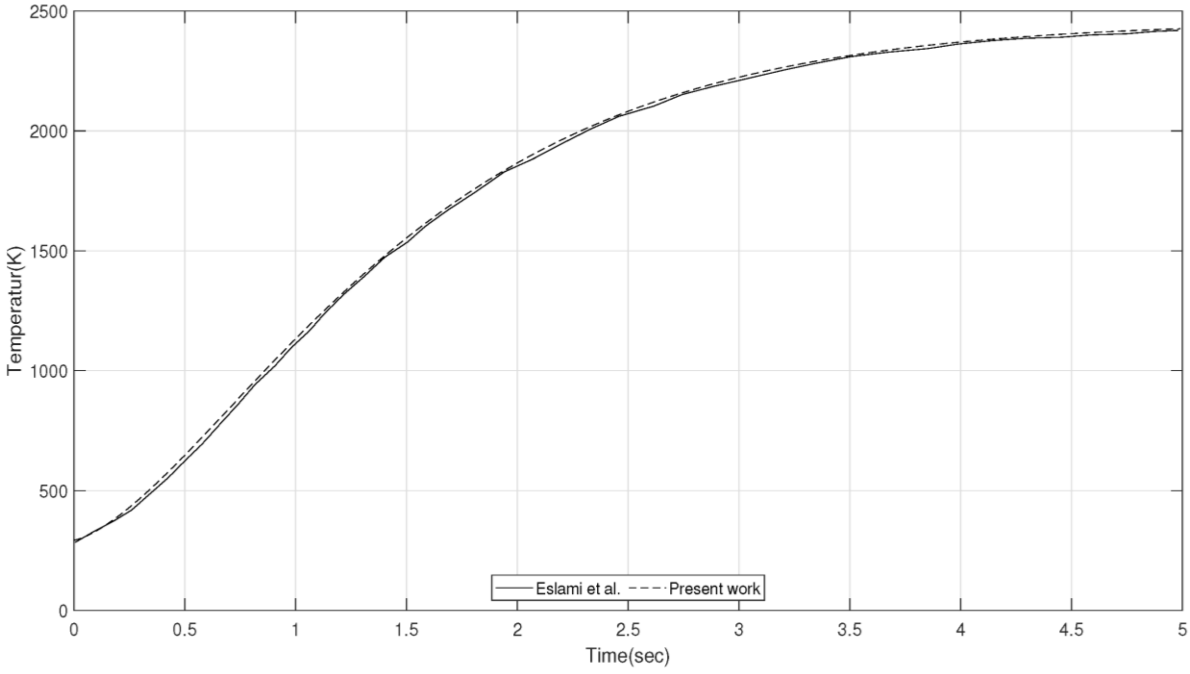

Figure 2 Temperature versus time for slow rate load.

In this formulation, *i* represents the power-law index, indicating the material variation throughout the shell thickness. The value of *i* is always greater than or equal to zero, with zero representing a fully metal composition and infinity representing a fully ceramic composition. It is important to note that we assume Poisson's ratio to be constant across the shell thickness due to its negligible variation within the constituent materials.

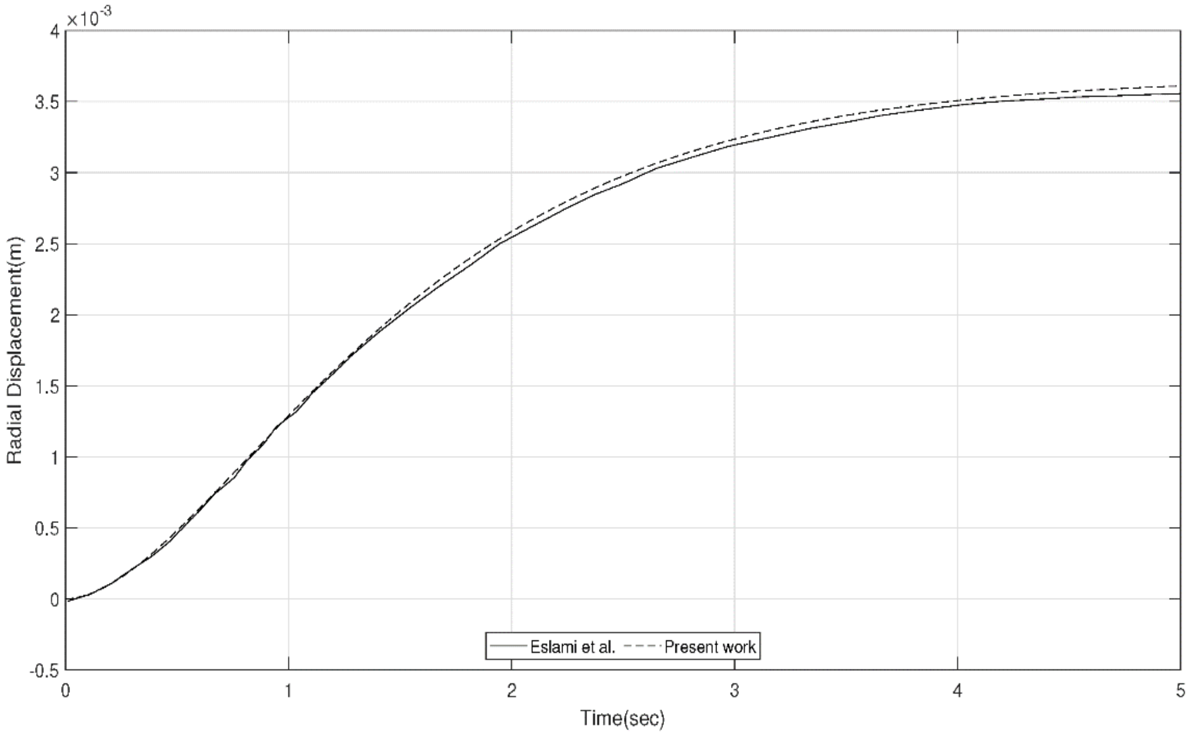

Figure 3 Applied thermal shock, case (1).

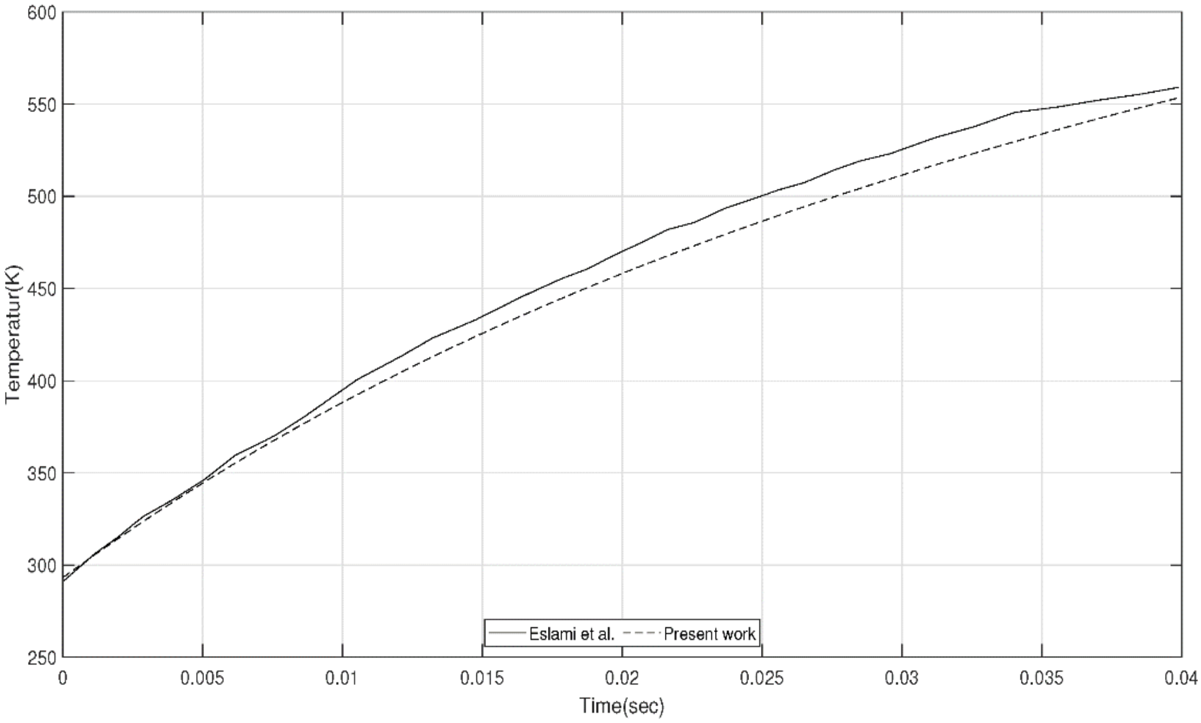

Figure 4 Temperature versus time for fast rate load.

2.1 Strain-displacement relations

The cylindrical coordinates (x, θ, z) are considered along the axial, circumferential, and normal to shell surface directions. The displacement components based on the first order approximation are represented as

$$
\begin{aligned}
u(x,\theta,z) &= u_0(x,\theta) + z\psi_x(x,\theta) \\
w(x,\theta,z) &= w_0(x,\theta)
\end{aligned}
\tag{5}
$$

where u_0 and w_0 represent the components of displacement vector on the middle plane of the shell at a point along the x and z-directions, respectively. The strain-displacement relations for the cylindrical shell based on the first order shear deformation theory are given as

$$
\begin{aligned}
\mathcal{E}_{xx} &= u_{0,x} + z\psi_{x,x} \\
\mathcal{E}_{\theta\theta} &= \frac{1}{1+\frac{z}{R}}\frac{w_0}{R} \\
\mathcal{E}_{xz} &= \frac{1}{2}\left(w_{0,x} + \psi_x\right)
\end{aligned}
\tag{6}
$$

2.2 Stress-strain relations

The stress-strain relations for a functionally graded shell based on the assumed displacement model, including the shear deformations, are

$$
\begin{aligned}
\sigma_{xx} &= \frac{E(z)}{1-\nu^2}[\varepsilon_{xx} + \nu\varepsilon_{\theta\theta}] - \frac{E(z)\alpha(z)}{1-\nu}(T - T_a) \\
\sigma_{\theta\theta} &= \frac{E(z)}{1-\nu^2}[\varepsilon_{\theta\theta} + \nu\varepsilon_{xx}] - \frac{E(z)\alpha(z)}{1-\nu}(T - T_a) \\
\tau_{xz} &= \frac{E(z)}{1+\nu}\varepsilon_{xz}
\end{aligned}
\tag{7}
$$

where T_a is the reference temperature. The force and moment resultants from the second order shell theory are

$$
\begin{aligned}
\begin{Bmatrix} N_{xx} \\ Q_x \end{Bmatrix} &= \int_z \begin{Bmatrix} \sigma_{xx} \\ \tau_{xz} \end{Bmatrix}\left(1 + \frac{z}{R}\right) dz \\
\{N_{\theta\theta}\} &= \int_z \{\sigma_{\theta\theta}\}\, dz \\
\{M_{xx}\} &= \int_z \{\sigma_{xx}\}\left(1 + \frac{z}{R}\right) dz
\end{aligned}
\tag{8}
$$

2.3 Equations of motion

The Hamilton principle obtains the following equations for the axisymmetric loading conditions in cylindrical coordinates, including the shear deformations.

$$\begin{aligned}\frac{\partial N_{xx}}{\partial x} &= I_0\ddot{u}_0 + I_1\ddot{\psi}_x \\ \frac{\partial Q_x}{\partial x} - \frac{N_{\theta\theta}}{R} &= I_0\ddot{w}_0 \\ \frac{\partial M_{xx}}{\partial x} &= I_1\ddot{u}_0 + I_2\ddot{\psi}_x\end{aligned} \tag{9}$$

where

$$I_{0,1,2} = \int_{-\frac{h}{2}}^{\frac{h}{2}} \rho(z)(1, z, z^2)dz \tag{10}$$

For the thin cylindrical shells, temperature distribution across the shell thickness may be assumed to be linear as

$$\Delta T(x,z,t) = T_0(x,t) + zT_1(x,t) \tag{11}$$

where T_0 and T_1 are the unknown functions to be obtained. Substituting Eqs. (5) into Eqs. (7) and using Eqs. (8) and (11) and finally substituting the resulting equations into the equations of motion (9), the equations of motion are obtained in terms of the displacement components as

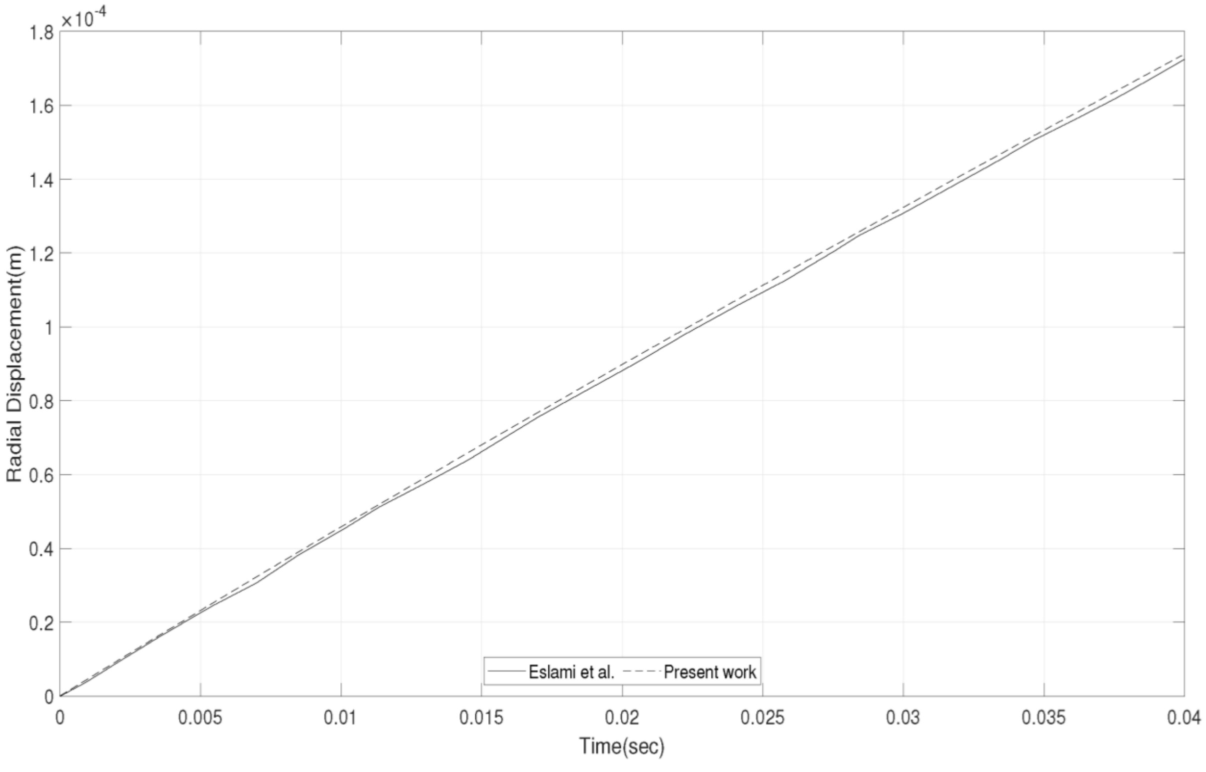

Figure 5 Radial displacement versus time for fast rate load.

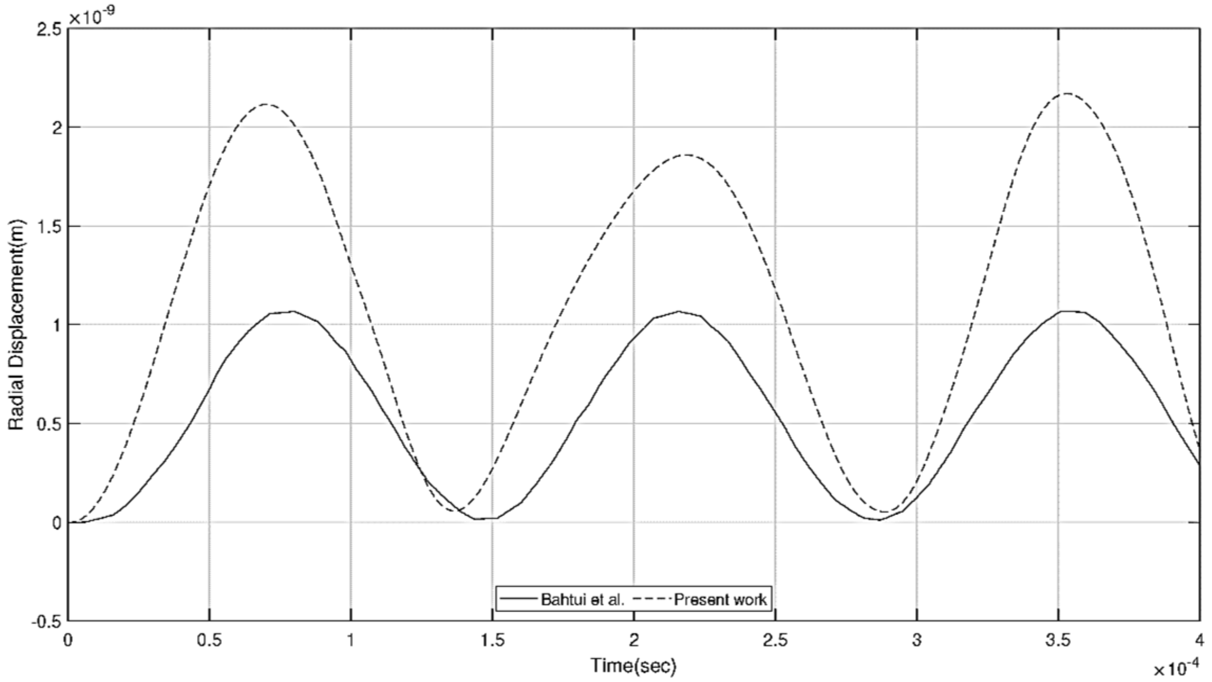

Figure 6 Radial displacement versus time.

$$A_3\frac{\partial^2 u_0}{\partial x^2}+A_1\frac{\partial w_0}{\partial x}+A_4\frac{\partial^2\psi_x}{\partial x^2}-B_3\frac{\partial T_0}{\partial x}-B_4\frac{\partial T_1}{\partial x}=I_0\ddot{u}_0+I_1\ddot{\psi}_x$$

$$\acute{A}_1\frac{\partial^2 w_0}{\partial x^2}+\acute{A}_1\frac{\partial\psi_x}{\partial x}-\left(A_1\frac{\partial u_0}{\partial x}+A_6 w_0+A_2\frac{\partial\psi_x}{\partial x}-B_1T_0-B_2T_1\right)=I_0\ddot{w}_0 \qquad (12)$$

$$A_4\frac{\partial^2 u_0}{\partial x^2}+A_2\frac{\partial w_0}{\partial x}+A_5\frac{\partial^2\psi_x}{\partial x^2}-B_4\frac{\partial T_0}{\partial x}-B_5\frac{\partial T_1}{\partial x}-\left(\acute{A}_1\frac{\partial w_0}{\partial x}+\acute{A}_1\psi_x\right)=I_0\ddot{u}_0+I_1\ddot{\psi}_x$$

where $\acute{A}_1$, $A_j(j = 1..6)$, and $B_i(j = 1..5)$ are constants given in the Appendix. Three equations of motion contain five unknown dependent functions u_0, w_0, ψ_x, T_0, and T_1. This means that two more equations are needed to complete the necessary equations and calculate the dependent functions. These two equations are derived by employing the energy equation.

2.4 Energy equation

The first law of thermodynamics for heat conduction equation is assumed for the functionally graded cylindrical shell. The classical theory of coupled thermoelasticity for the FGM cylindrical shell is considered as [1]

$$\rho c_\epsilon\dot{T}+\overline{\beta}T_a\dot{\varepsilon}_{ii}=\left(kT_{,i}\right)_{,i} \qquad (11)$$

where ρ is the mass density, c_ϵ is the specific heat at constant strain, $\overline{\beta}=E\alpha/(1-2\nu)$, T_a is the reference temperature, and k is the heat conduction coefficient. This equation may be written in expanded form for the assumed conditions. We move all parts of the equation to the left side of the equation and call it the residue Re. The resulting residue Re is made orthogonal with respect to 1 and z. This yields two independent equations for T_0 and T_1, as it is made orthogonal with respect to 1 and z for T_0 and T_1 [2]

$$\int_{-h/2}^{h/2} Re \times dz = 0$$

$$\int_{-h/2}^{h/2} Re \times zdz = 0 \tag{14}$$

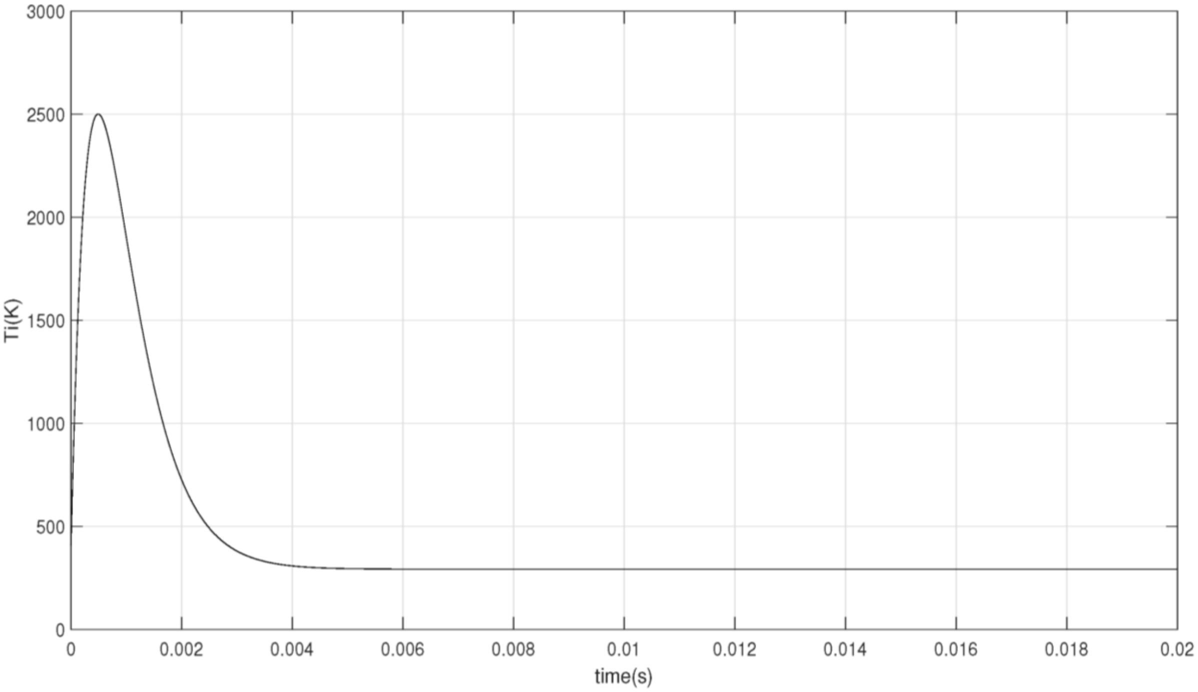

Figure 7 Applied thermal shock, case (1).

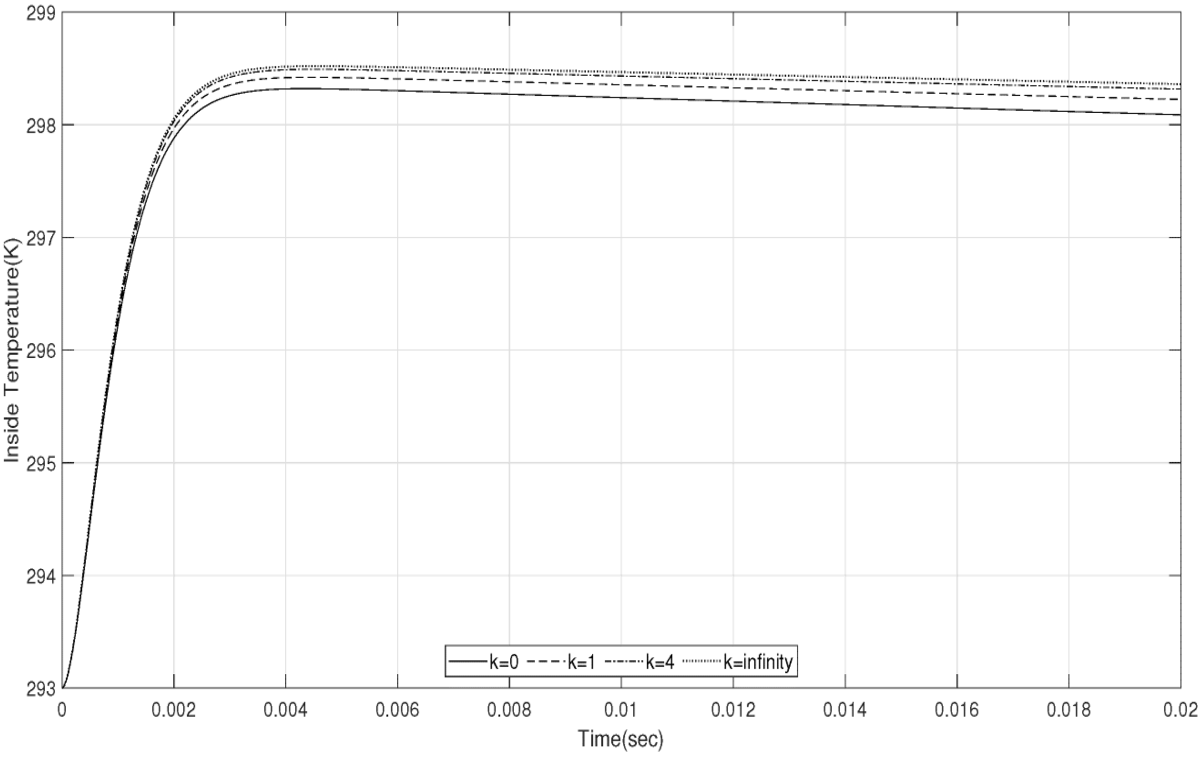

Figure 8 Inside temperature of the shell at $x = 225\ mm$ versus time for different power law indices, case (1).

Five governing equations, including the equations of motion and the energy equations, must be simultaneously solved to obtain the displacements and temperature functions.
As the thermal boundary conditions, it is considered that the heat flux Q_{in} and Q_{out} are applied on the inside and outside surfaces of the shell

$$k(-h/2)\left.\frac{\partial T}{\partial z}\right|_{-\frac{h}{2}} = h_{in}\left(T - T_{\infty}^{in}\right), \qquad z = -\frac{h}{2} \tag{15}$$

$$k(h/2)\left.\frac{\partial T}{\partial z}\right|_{\frac{h}{2}} = h_{in}\left(T - T_{\infty}^{out}\right), \qquad z = \frac{h}{2} \tag{16}$$

Using Eqs. (11) and (14) for the linear approximation of temperature distribution across the thickness direction, two energy equations for the cylindrical shell are obtained as

$$\begin{aligned}&\acute{B}_1\frac{\partial \dot{u}_0}{\partial x} + \acute{B}_2\frac{\partial \dot{\psi}_x}{\partial x} + F_1\dot{T}_0 + F_2\dot{T}_1 - D_1\frac{\partial^2 T_0}{\partial x^2} - D_2\frac{\partial^2 T_1}{\partial x^2} - D_4 T_1 + h_{in}\left(T_0 - \frac{h}{2}T_1\right)\\&\qquad + h_{out}\left(T_0 + \frac{h}{2}T_1\right) = h_{in}\left(T_{in}(t) - T_a\right)\\&\acute{B}_2\frac{\partial \dot{u}_0}{\partial x} + \acute{B}_5\dot{w} + \acute{B}_3\frac{\partial \dot{\psi}_x}{\partial x} + F_2\dot{T}_0 + F_3\dot{T}_1 - D_2\frac{\partial^2 T_0}{\partial x^2} - D_3\frac{\partial^2 T_1}{\partial x^2} + D_5 T_1\\&\qquad - \frac{h}{2}h_{in}\left(T_0 - \frac{h}{2}T_1\right) - \frac{h}{2}h_{out}\left(T_0 + \frac{h}{2}T_1\right) = -\frac{h}{2}h_{in}\left(T_{in}(t) - T_a\right)\end{aligned} \tag{17}$$

where the constants $F_j(j = 1..3)$, $\acute{B}_i$, $D_i(j = 1..5)$ are given in the Appendix.

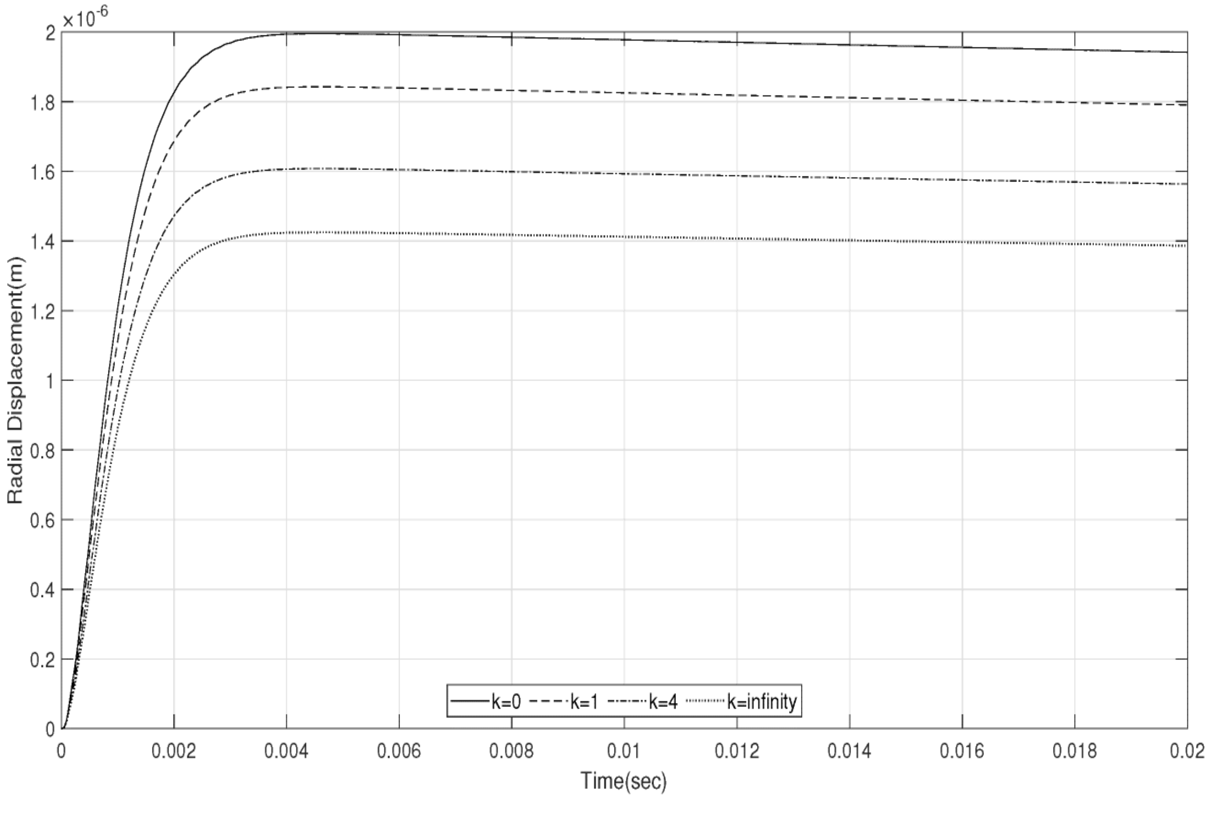

Figure 9 Radial displacement of the shell at $x = 225\ mm$ versus time for different power law indices, case (1).

2.5 Numerical solution

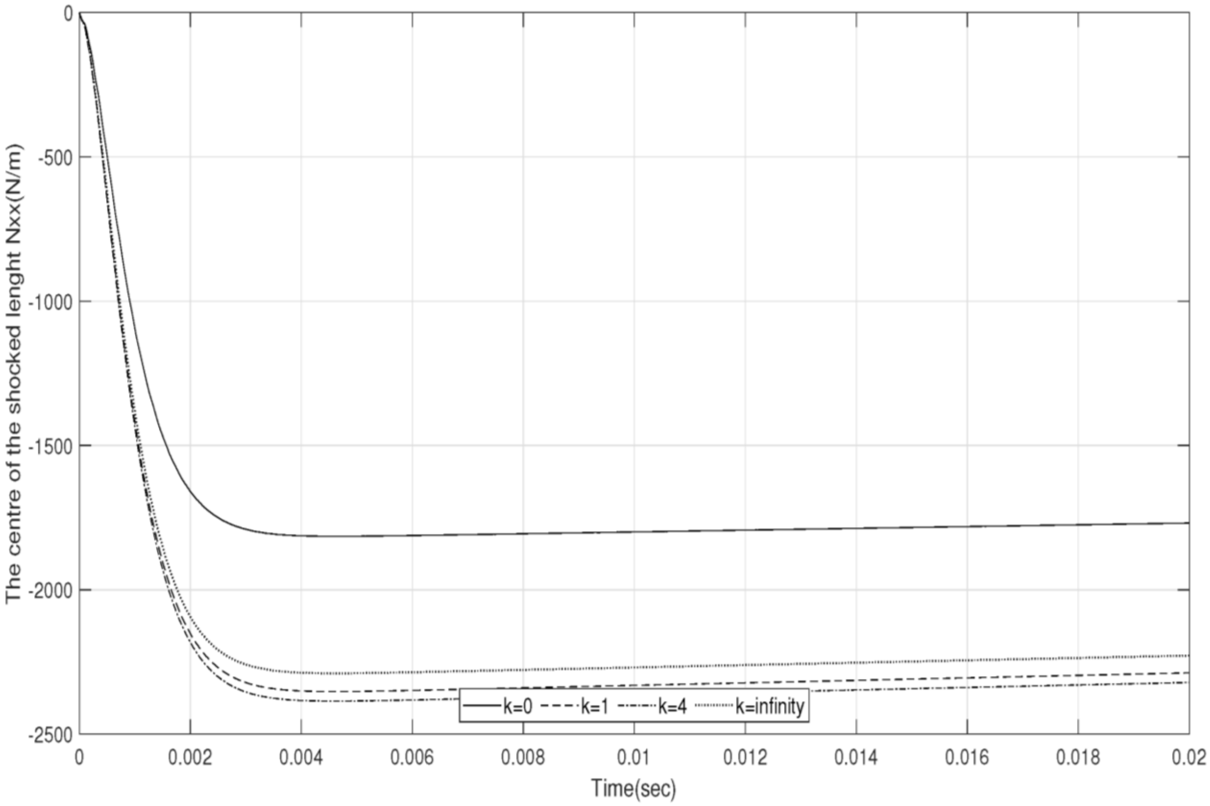

Figure 10 Axial force resultant of the shell at $x = 225\ mm$ versus time, case (1).

Consider a cylindrical shell under axisymmetric partial thermal shock load. Temperature distribution across the shell thickness is assumed to be linear. Under such assumed conditions five unknown functions u_0, u_0, ψ_x, T_0, T_1, as given by Eqs. (12) and (17), appear in the governing equations. These equations are transformed into the dimensionless form by the following dimensionless parameters

$$\bar{x} = \frac{x}{x_c} = \frac{1}{l}x, \qquad \bar{t} = \frac{t}{t_c} = \frac{c_1}{l}t, \qquad \bar{T}_0 = \frac{T_0}{T_{0c}} = \frac{1}{T_a}T_0, \qquad \bar{T}_1 = \frac{T_1}{T_{1c}} = \frac{1}{T_a}T_1,$$
$$\bar{u}_0 = \frac{u_0}{u_c} = \frac{1}{l\alpha_m T_a}u_0, \qquad \bar{w}_0 = \frac{w_0}{w_c} = \frac{1}{l\alpha_m T_a}w_0, \tag{18}$$
$$\bar{\psi}_x = \frac{\psi_x}{\psi_c} = \frac{1}{\alpha_m T_a}\psi_0$$

where

$$c_1 = \sqrt{\frac{E_m}{(1-\nu^2)\rho_m}}$$
$$l = \frac{k_m}{\rho_m c_m c_1}$$

Here, the subscript m denotes the material properties of metal constituent. With the assumed dimensionless parameters, consider the quadratic shape function for the base element (e) of the dependent functions as

$$\begin{aligned}
\bar{u}_0^{(e)}(x) &= \langle N_1 \quad N_2 \quad N_3 \rangle^{(e)} \begin{Bmatrix} \bar{u}_{01} \\ \bar{u}_{02} \\ \bar{u}_{03} \end{Bmatrix}^{(e)} \\
\bar{w}_0^{(e)}(x) &= \langle N_1 \quad N_2 \quad N_3 \rangle^{(e)} \begin{Bmatrix} \bar{w}_{01} \\ \bar{w}_{02} \\ \bar{w}_{03} \end{Bmatrix}^{(e)} \\
\bar{\psi}_x^{(e)}(x) &= \langle N_1 \quad N_2 \quad N_3 \rangle^{(e)} \begin{Bmatrix} \bar{\psi}_{x1} \\ \bar{\psi}_{x2} \\ \bar{\psi}_{x3} \end{Bmatrix}^{(e)} \\
\bar{T}_0^{(e)}(x) &= \langle N_1 \quad N_2 \quad N_3 \rangle^{(e)} \begin{Bmatrix} \bar{T}_{01} \\ \bar{T}_{02} \\ \bar{T}_{03} \end{Bmatrix}^{(e)} \\
\bar{T}_1^{(e)}(x) &= \langle N_1 \quad N_2 \quad N_3 \rangle^{(e)} \begin{Bmatrix} \bar{T}_{11} \\ \bar{T}_{12} \\ \bar{T}_{13} \end{Bmatrix}^{(e)}
\end{aligned} \tag{19}$$

where

$$\begin{aligned}
N_1(\bar{x}) &= \left(1 - 2\frac{\bar{x}}{L^{(e)}}\right)\left(1 - \frac{\bar{x}}{L^{(e)}}\right) \\
N_2(\bar{x}) &= 4\frac{\bar{x}}{L^{(e)}}\left(1 - \frac{\bar{x}}{L^{(e)}}\right) \\
N_3(\bar{x}) &= -\frac{\bar{x}}{L^{(e)}}\left(1 - 2\frac{\bar{x}}{L^{(e)}}\right)
\end{aligned} \tag{20}$$

and, $\bar{L}^{(e)}$ being the length of base element (e). Applying the Galerkin method to the system of five equations and employing the weak formulations, yield

$$\begin{aligned}
\int\limits_{\bar{L}^{(e)}} \Bigg[& A_3 \frac{u_c}{x_c^2} \frac{\partial N_m}{\partial \bar{x}} \frac{\partial N_i}{\partial \bar{x}} \bar{u}_{0i} + A_1 \frac{w_c}{x_c} \frac{\partial N_m}{\partial \bar{x}} N_i \bar{w}_{0i} + A_4 \frac{\psi_c}{x_c^2} \frac{\partial N_m}{\partial \bar{x}} \frac{\partial N_i}{\partial \bar{x}} \bar{\psi}_{xi} \\
& - B_3 \frac{T_{0c}}{x_c} \frac{\partial N_m}{\partial \bar{x}} N_i \bar{T}_{0i} - B_4 \frac{T_{1c}}{x_c} \frac{\partial N_m}{\partial \bar{x}} N_i \bar{T}_{1i} + I_0 \frac{u_c}{t_c^2} N_m N_i \ddot{\bar{u}}_{0i} \\
& + I_1 \frac{\psi_c}{t_c^2} N_m N_i \ddot{\bar{\psi}}_{xi} \Bigg] d\bar{x} = N_{xx} N_m \big|_0^L
\end{aligned}$$

$$\begin{aligned}
\int\limits_{\bar{L}^{(e)}} \Bigg[& A_1 \frac{u_c}{x_c} N_m \frac{\partial N_i}{\partial \bar{x}} \bar{u}_{0i} + \left(\acute{A}_1 \frac{w_c}{x_c^2} \frac{\partial N_m}{\partial \bar{x}} \frac{\partial N_i}{\partial \bar{x}} + A_6 w_c N_m N_i \right) \bar{w}_{0i} \\
& + \left(\acute{A}_1 \frac{\psi_c}{x_c^2} \frac{\partial N_m}{\partial \bar{x}} N_i + A_2 \frac{\psi_c}{x_c} N_m \frac{\partial N_i}{\partial \bar{x}} \right) \bar{\psi}_{xi} - B_1 T_{0c} N_m N_i \bar{T}_{0i} \\
& - B_2 T_{1c} N_m N_i \bar{T}_{1i} + I_0 \frac{w_c}{t_c^2} N_m N_i \ddot{\bar{w}}_{0i} \Bigg] d\bar{x} = Q_{xx} N_m \big|_0^L
\end{aligned}$$

$$\begin{aligned}
&\int_{\bar{L}^{(e)}} \Bigg[A_4 \frac{u_c}{x_c^2}\frac{\partial N_m}{\partial \bar{x}}\frac{\partial N_i}{\partial \bar{x}}\bar{u}_{0i} + \left(A_2 \frac{w_c}{x_c}\frac{\partial N_m}{\partial \bar{x}} N_i + \acute{A}_1 \frac{w_c}{x_c} N_m \frac{\partial N_i}{\partial \bar{x}}\right)\bar{w}_{0i} \\
&\qquad + \left(A_5 \frac{\psi_c}{x_c^2}\frac{\partial N_m}{\partial \bar{x}}\frac{\partial N_i}{\partial \bar{x}} + \acute{A}_1 \psi_c N_m N_i\right)\bar{\psi}_{xi} - B_4 \frac{T_{0c}}{x_c}\frac{\partial N_m}{\partial \bar{x}} N_i \bar{T}_{0i} \\
&\qquad - B_5 \frac{T_{1c}}{x_c}\frac{\partial N_m}{\partial \bar{x}} N_i \bar{T}_{1i} + \left(I_1 \frac{u_c}{t_c^2} N_m N_i \ddot{\bar{u}}_{0i} + I_2 \frac{\psi_c}{t_c^2} N_m N_i \ddot{\bar{\psi}}_{xi}\right)\Bigg] d\bar{x} \\
&\qquad = M_{xx} N_m\big|_0^L
\end{aligned} \tag{21}$$

$$\begin{aligned}
&\int_{\bar{L}^{(e)}} \Bigg[\acute{B}_1 \frac{u_c}{x_c t_c} N_m \frac{\partial N_i}{\partial \bar{x}}\dot{\bar{u}}_{0i} + \acute{B}_4 \frac{w_c}{t_c} N_m N_i \dot{\bar{w}}_{0i} + \acute{B}_2 \frac{\psi_c}{x_c t_c} N_m \frac{\partial N_i}{\partial \bar{x}}\dot{\bar{\psi}}_{xi} + F_1 \frac{T_{0c}}{t_c} N_m N_i \dot{\bar{T}}_{0i} \\
&\qquad + F_2 \frac{T_{1c}}{t_c} N_m N_i \dot{\bar{T}}_{1i} - \left(D_1 \frac{T_{0c}}{x_c^2} N_m \frac{\partial^2 N_i}{\partial \bar{x}^2} - T_{0c}(h_{in} + h_{out}) N_m N_i\right)\bar{T}_{0i} \\
&\qquad - \Bigg(D_4 T_{1c} N_m N_i + D_2 \frac{T_{1c}}{x_c^2} N_m \frac{\partial^2 N_i}{\partial \bar{x}^2} \\
&\qquad - \frac{h}{2} T_{1c}(-h_{in} + h_{out}) N_m N_i\Bigg)\bar{T}_{1i}\Bigg] d\bar{x} = \int_{\bar{L}^{(e)}} h_{in}(T_{in}(t) - T_a) N_m d\bar{x}
\end{aligned}$$

$$\begin{aligned}
&\int_{\bar{L}^{(e)}} \Bigg[\acute{B}_2 \frac{u_c}{x_c t_c} N_m \frac{\partial N_i}{\partial \bar{x}}\dot{\bar{u}}_{0i} + \acute{B}_5 \frac{w_c}{t_c} N_m N_i \dot{\bar{w}}_{0i} + \acute{B}_3 \frac{\psi_c}{x_c t_c} N_m \frac{\partial N_i}{\partial \bar{x}}\dot{\bar{\psi}}_{xi} + F_2 \frac{T_{0c}}{t_c} N_m N_i \dot{\bar{T}}_{0i} \\
&\qquad + F_3 \frac{T_{1c}}{t_c} N_m N_i \dot{\bar{T}}_{1i} - \left(D_2 \frac{T_{0c}}{x_c^2} N_m \frac{\partial^2 N_i}{\partial \bar{x}^2} + \frac{h}{2} T_{0c}(h_{in} + h_{out}) N_m N_i\right)\bar{T}_{0i} \\
&\qquad - \Bigg(-D_5 T_{1c} N_m N_i + D_3 \frac{T_{1c}}{x_c^2} N_m \frac{\partial^2 N_i}{\partial \bar{x}^2} \\
&\qquad - \frac{h^2}{4} T_{1c}(h_{in} - h_{out}) N_m N_i\Bigg)\bar{T}_{1i}\Bigg] d\bar{x} = \int_{\bar{L}^{(e)}} -\frac{h}{2} h_{in}(T_{in}(t) - T_a) N_m d\bar{x}
\end{aligned}$$

where $T_{in}(t)$ is the applied thermal shock. Set of Eqs. (21) are assembled for all the finite elements of the solution domain and the final equation is given as

$$[\mathrm{M}]\{\ddot{X}\} + [C]\{\dot{X}\} + [K]\{X\} = \{F(t)\} \tag{22}$$

where $[M]$, $[C]$, and $[K]$ are the global mass, damping, and stiffness matrix. The matrix $\{F(t)\}$ is the global force matrix and $\{X\}$ is the global unknown matrix in form of the non-dimensional displacement components defined by Eqs. (19). The finite element equation of (22) maybe solved in time domain by many techniques. In this paper, the Newmark method is used. In this technique, the velocity and acceleration matrices at time $t + \Delta t$ are approximated in terms of their values at time t as [19]

$$\begin{aligned}
\{\dot{X}\}_{t+\Delta t} &= \frac{\alpha}{\beta \Delta t}(\{X\}_{t+\Delta t} - \{X\}_t) + \left(1 - \frac{\alpha}{\beta}\right)\{\dot{X}\}_t + \left(1 - \frac{\alpha}{2\beta}\right)\Delta t \{\ddot{X}\}_t \\
\{\ddot{X}\}_{t+\Delta t} &= \frac{1}{\beta \Delta t^2}(\{X\}_{t+\Delta t} - \{X\}_t) - \frac{1}{\beta \Delta t}\{\dot{X}\}_t + \left(1 - \frac{1}{2\beta}\right)\{\ddot{X}\}_t
\end{aligned} \tag{23}$$

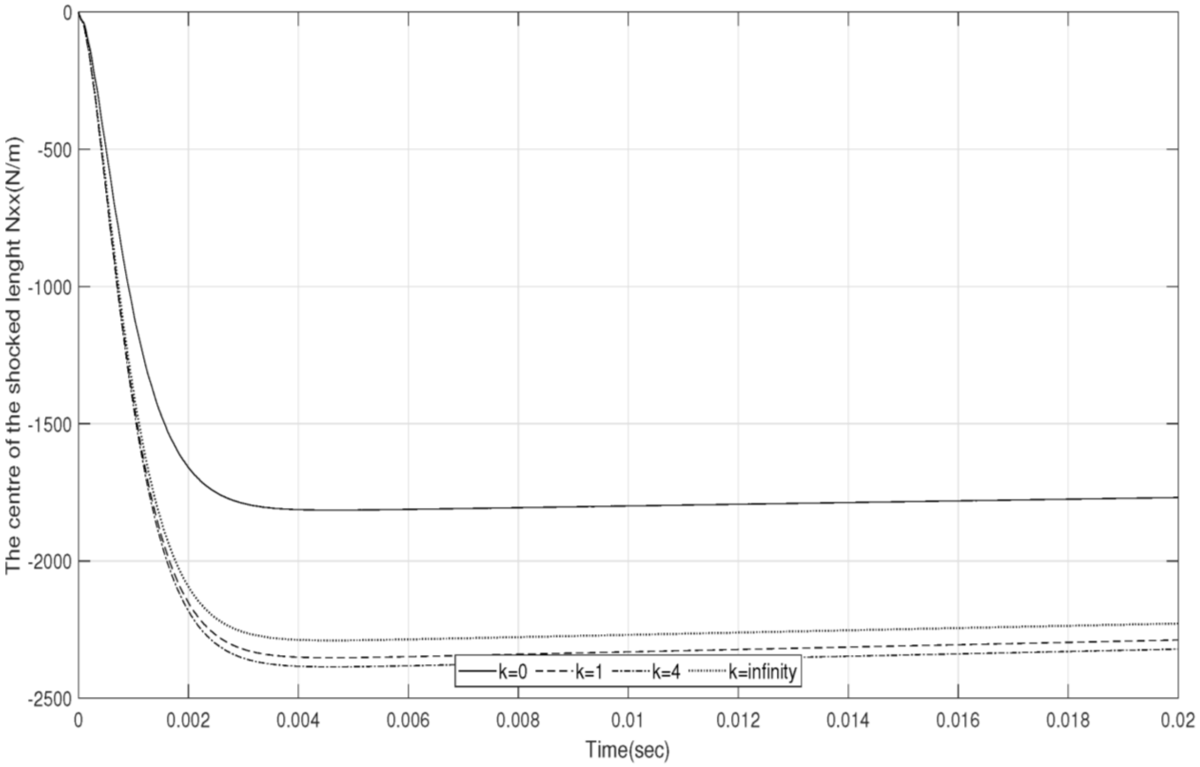

Figure 11 Axial force resultant of the shell at $x = 225\ mm$ versus time, case (1).

where the coefficients α and β are parameters which determine the accuracy and stability of the numerical technique. For time $t + \Delta t$, we get

$$[\widehat{K}]\{X\}_{t+\Delta t} = \{\widehat{F}\} \tag{24}$$

where

$$[\widehat{K}] = \left[\frac{1}{\beta \Delta t^2}[M] + \frac{\alpha}{\beta \Delta t}[C] + [K]\right]$$

$$\begin{aligned} \{\widehat{F}\} = \{F\}_{t+\Delta t} + [M]\left(\frac{1}{\beta \Delta t^2}\{X\}_t + \frac{1}{\beta \Delta t}\{\dot{X}\}_t + \left(\frac{1}{2\beta} - 1\right)\{\ddot{X}\}_t\right) \\ + [C]\left(\frac{\alpha}{\beta \Delta t}\{X\}_t + \left(\frac{\alpha}{\beta} - 1\right)\{\dot{X}\}_t + \left(\frac{1}{2\beta} - 1\right)\Delta t\{\ddot{X}\}_t\right) \end{aligned} \tag{25}$$

3 Results and discussion

3.1 Verification

The present analysis is validated by results of Eslami et al. [6] and Bahtui et al. [20]. In both named paper, thermal shock is applied to inside surface of cylindrical shell but dimensions, material and heat flux rate are different. As seen in Figures (2-5) Errors of the temperature and radial displacement results for slow rate load $\left(\Delta T = 2207(1 - e^{-1.31t})\right)$ and fast rate load $\left(\Delta T = 2207(1 - e^{-13100t})\right)$ are less than 2 percent that is because of different shell theories considered. Bahtui et al. [20] applied impact heat flux with very fast rate ($\Delta T = 2201.85 \times ate^{-13100bt}$) that occur lateral vibration. As shown in Figure (6) different between frequencies is less than 4 percent but it is about 100 percent for amplitude.

These errors exist due to the difference of 36 percent between coefficients in stress-strain relations and 100 percent in the coupling coefficient.

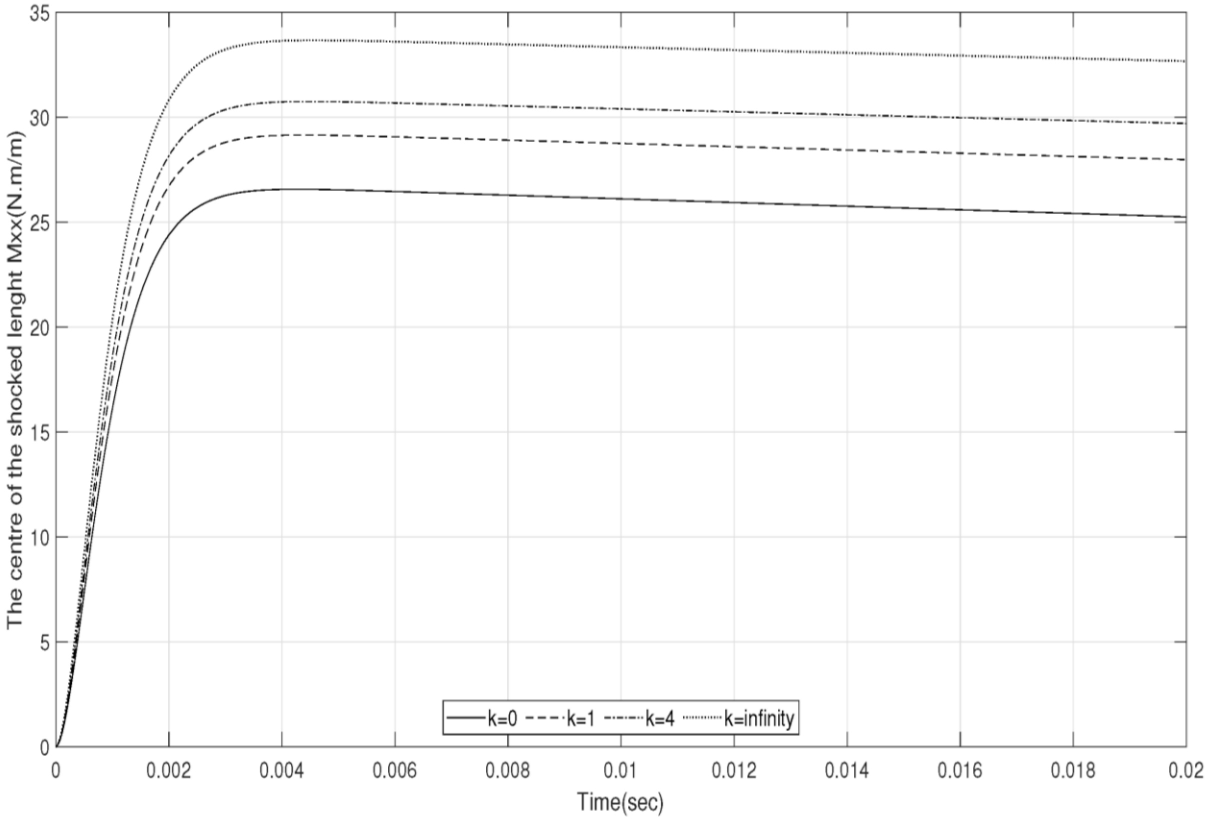

Figure 12 Axial moment resultant of the shell at $x = 225\ mm$ versus time, case (1).

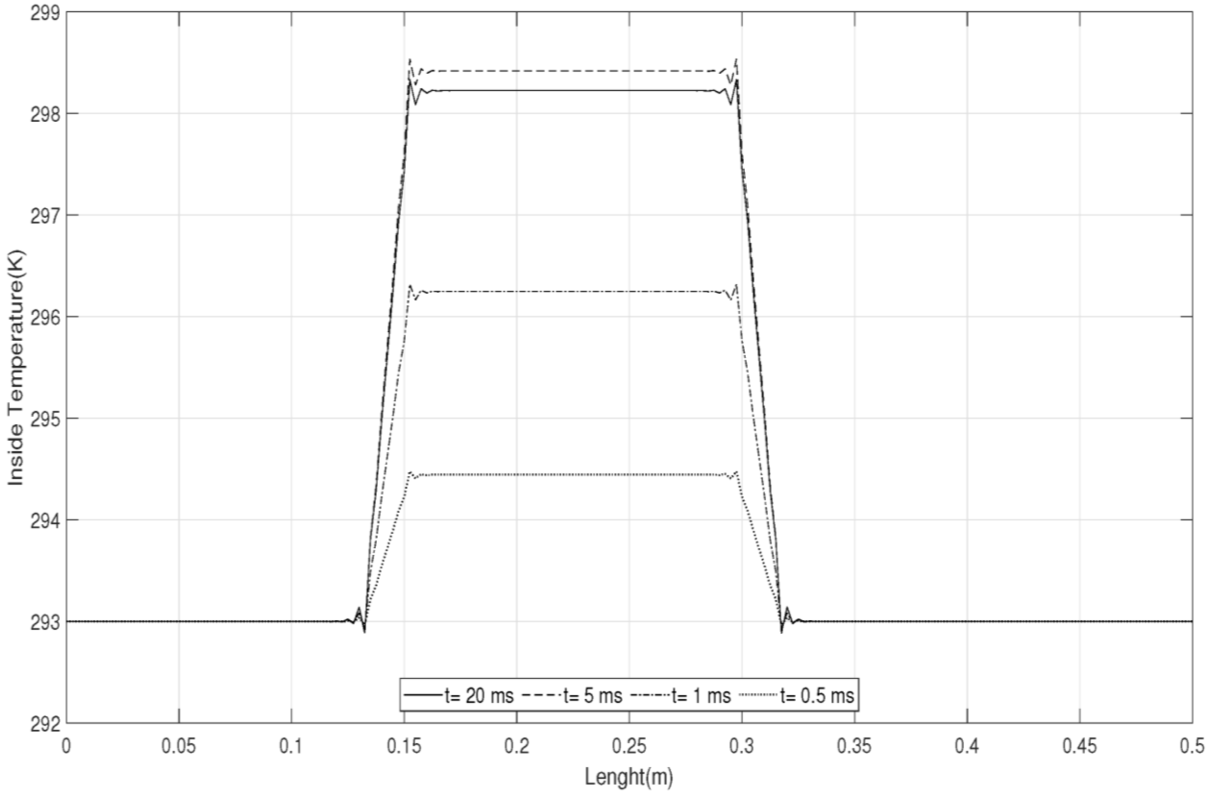

Figure 13 Variation of inside temperature versus shell length at different times, $k = 1$, case (1).

3.2 Results

Consider a simply supported functionally graded cylindrical shell under the inside axisymmetric partial thermal shock. The length, diameter and thickness of shell are 500 mm, 125 mm and 6.25 mm respectively. The functionally graded shell is assumed to be made of combination of metal (Ti–6Al–4V) and ceramic (ZrO2), at the initial temperature 298.15◦K, with the material properties shown in Table (1).

The shell is ceramic-rich at the inside and metal-rich at the outside surfaces, respectively. Temperature field across the shell thickness is assumed to be of linear type. Thermal shock is applied to the inside surface in the interval of $150mm \leq x \leq 300mm$ for two cases, which is shown in figures (7) and (16) The lowest natural frequency of the mentioned cylindrical shell for first mode in axial and circumferential direction is 5200 cycle/s [21] therefor it's period time is 0.192 ms. In case one applied temperature increase to maximum amount in 0.5 ms that is lower than period time of the cylindrical shell but in case two it's 0.05 ms.

For both cases, the boundary conditions at the ends of the shell are assumed to be thermally insulated and also the number of the elements is 60. Figure (8) shows the temperature of the shell at $x = 225\,mm$ versus time. This figure shows that for pure ceramic shell $(k = \infty)$, temperature distribution becomes higher, as the ceramic conductivity is lower compared to metal.

Table 1 Material properties of functionally graded constituent materials.

Metal	**Ceramic**
$E_m = 66.2\ Gpa$	$E_c = 117\ Gpa$
$\alpha_m = 10.3 \times 10^{-6}(1/K)$	$\alpha_c = 7.11 \times 10^{-6}(1/K)$
$\rho_m = 4.41 \times 10^{3}(kg/m^{3})$	$\rho_c = 5.6 \times 10^{3}(kg/m^{3})$
$k_m = 18.1(W/mK)$	$k_c = 2.036(W/mK)$
$c_m = 808.3(J/kg.K)$	$c_c = 615.6(J/kg.K)$
$\nu = 0.321$	$\nu = 0.333$

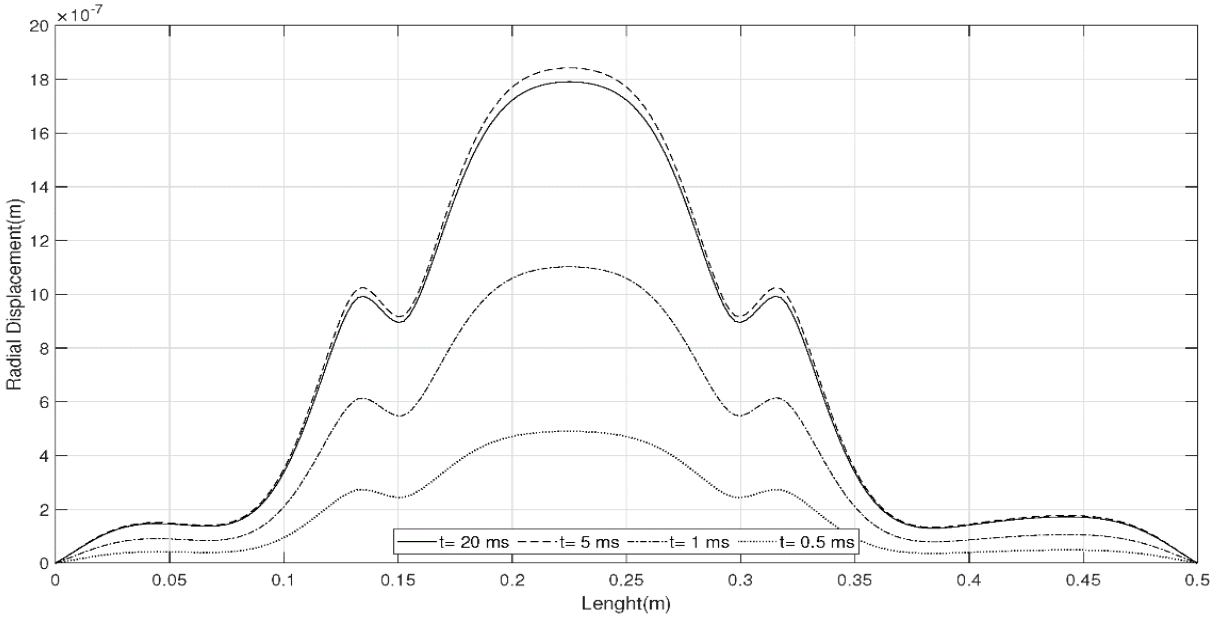

Figure 14 Variation of radial displacement versus shell length at different times, $k = 1$, case (1).

The lateral deflection of the shell at $x = 225\ mm$ versus time for different values of the power law index is shown in Figure (9). Since the thermal expansion coefficient of metal is larger than ceramic, as k increases, the lateral deflection increases. Figure (10) shows the axial force of the shell at $x = 225mm$ length versus time. The axial moment of the shell which is shown in Figure (11) increases as the metal volume fraction increase.

The variations of inside temperature, radial displacement, force and moment versus shell length are shown in Figures (12-15). In these diagrams, the index k is considered constant and is equal to $k = 1$. These diagrams are plotted at four specific moments of the solution time. Some errors in $x = 150\ mm$ and $x = 300\ mm$ areas are caused by discontinuity of applied thermal shock. In the second case, the shock load is ten times faster than in case one, and lateral vibration appears, as seen in Figure (18). Inside temperature versus time displayed in Figure (17), since the heat conduction coefficient of ceramic is higher than metal, as power law index k increases, inside temperature increases. The frequency of lateral vibration of the shell due to the increase of young modulus, as shown in Figure (18), increased. Also, the displacement amplitude decreases by increase of index k. The axial force for pure metal is lower than pure ceramic, and for FGM, it's higher than both, as illustrated in Figure (19). The axial moment versus time for different power law indexes, k is indicated in Figure (20). The results are compared for different coupling coefficients and demonstrated in Figures (21-24). For $\beta = 0$, the mechanical coupling term from the energy equation equals zero, and the problem is decoupled. By increasing the coupling coefficient, the effects of damping increase, as demonstrated in Figure (22). The axial force by increasing coupling coefficient decreases, as illustrated in Figure (23), but the axial moment does not change much, as shown in Figure (24).

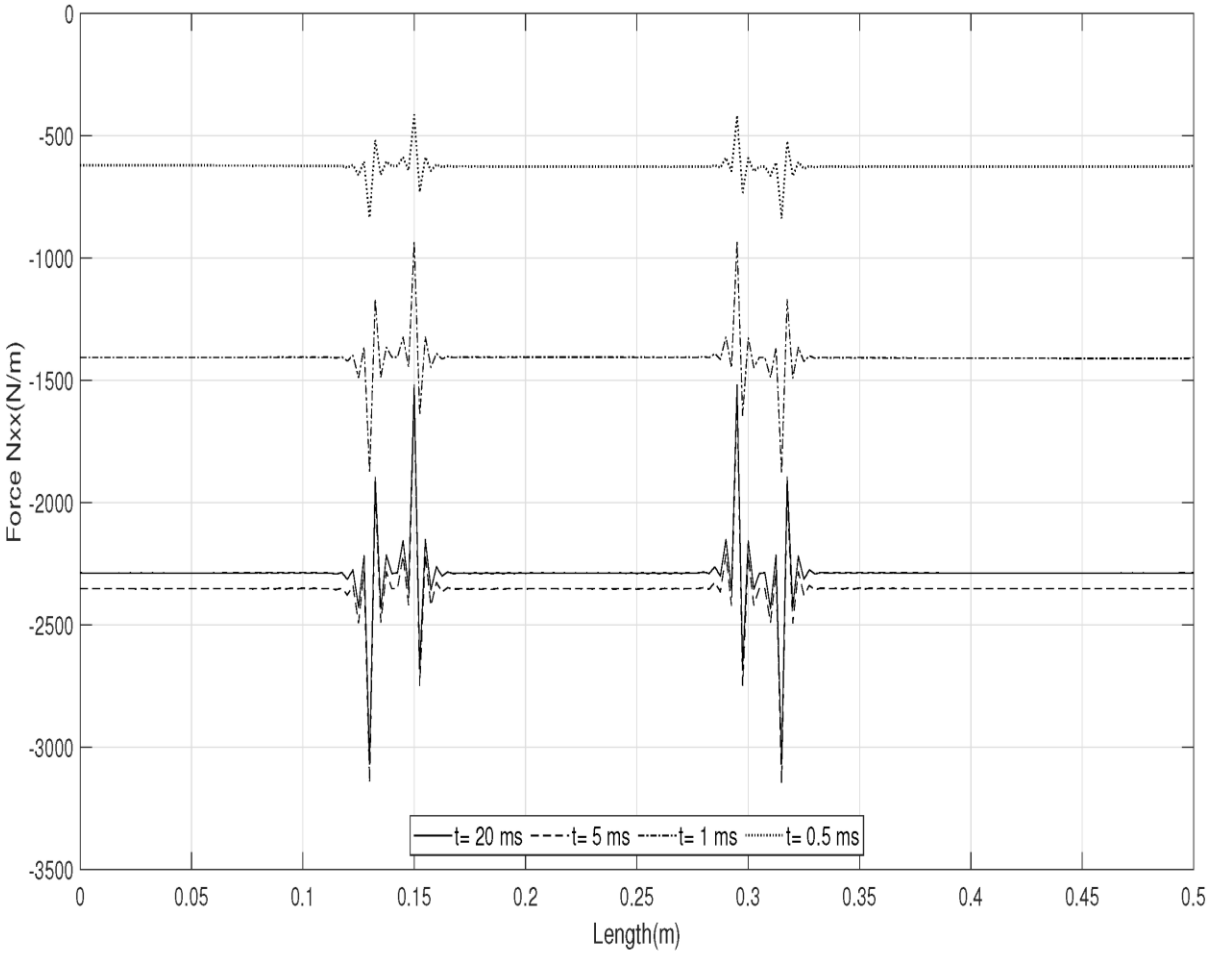

Figure 15 Variation of force resultant versus shell length at different times, $k = 1$, case (1).

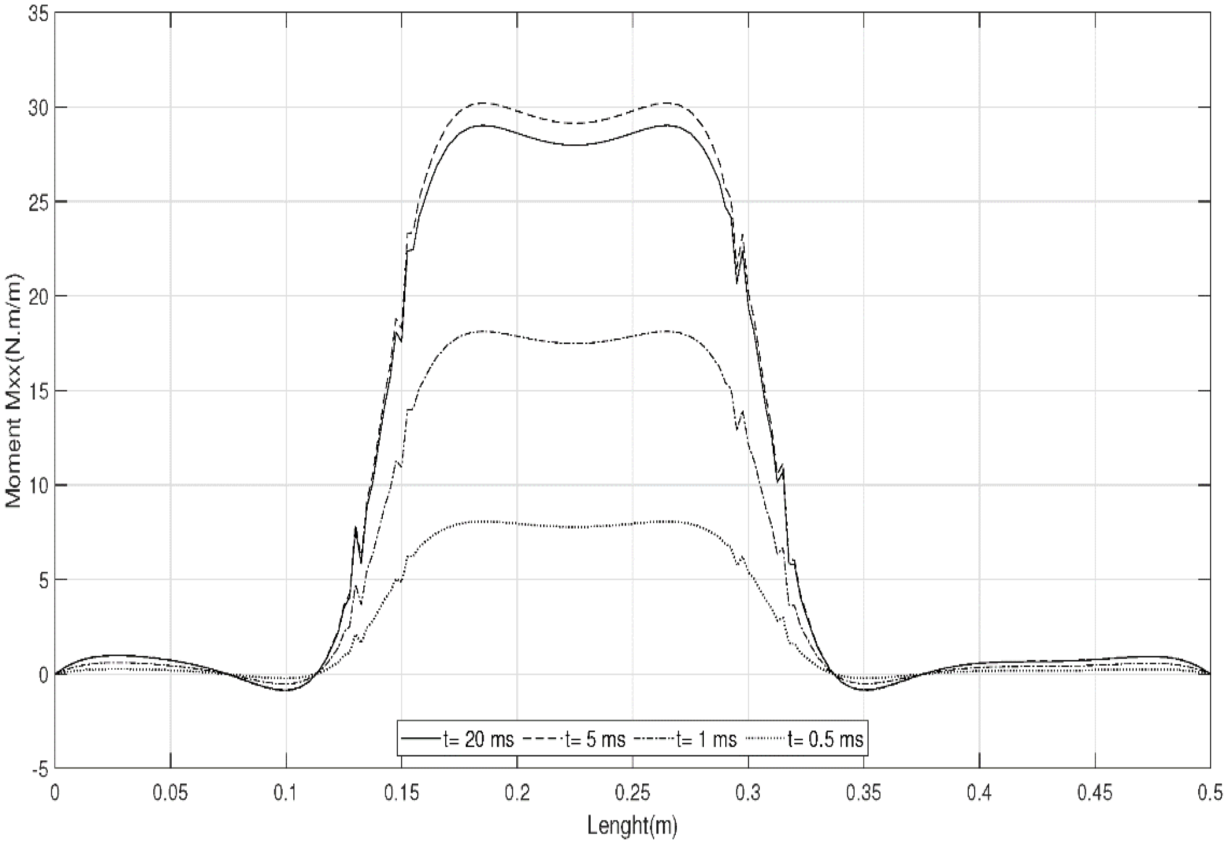

Figure 16 Variation of moment resultant versus shell length at different times, $k = 1$, case (1).

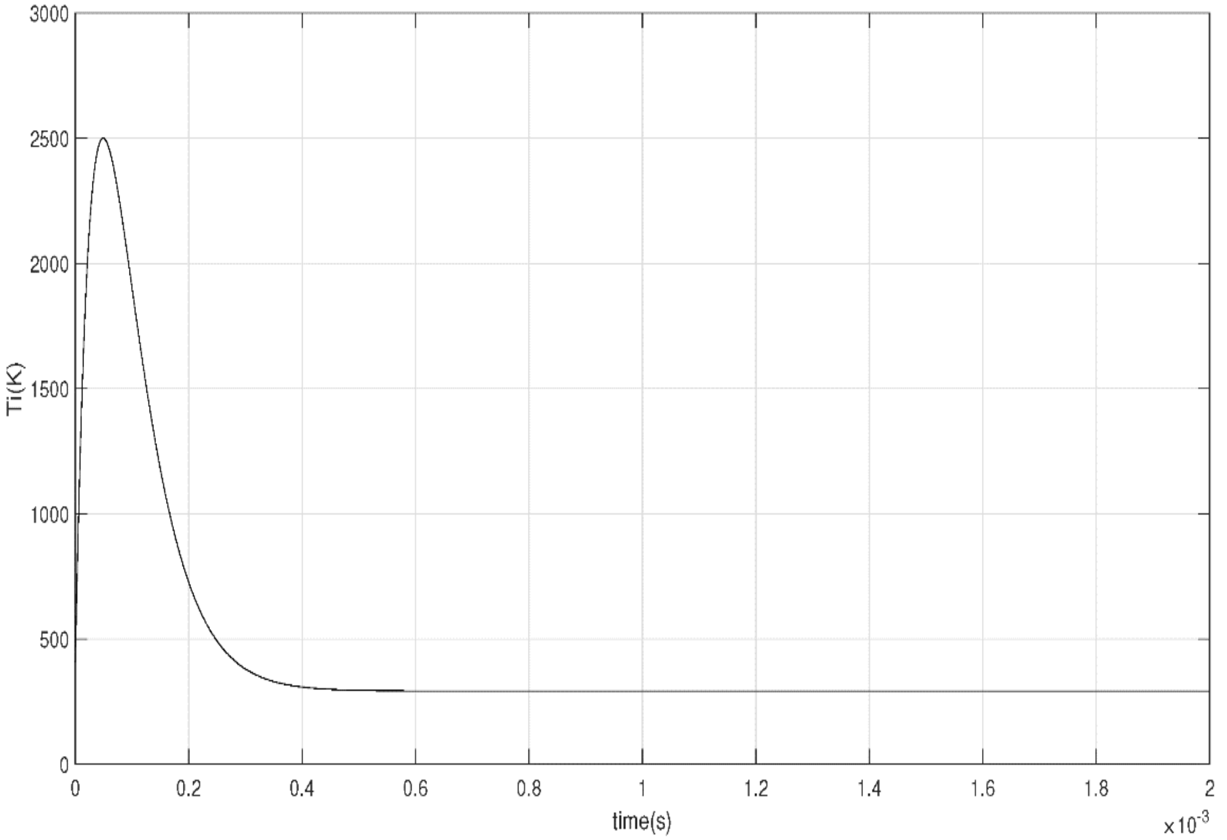

Figure 17 Applied thermal shock, case (2).

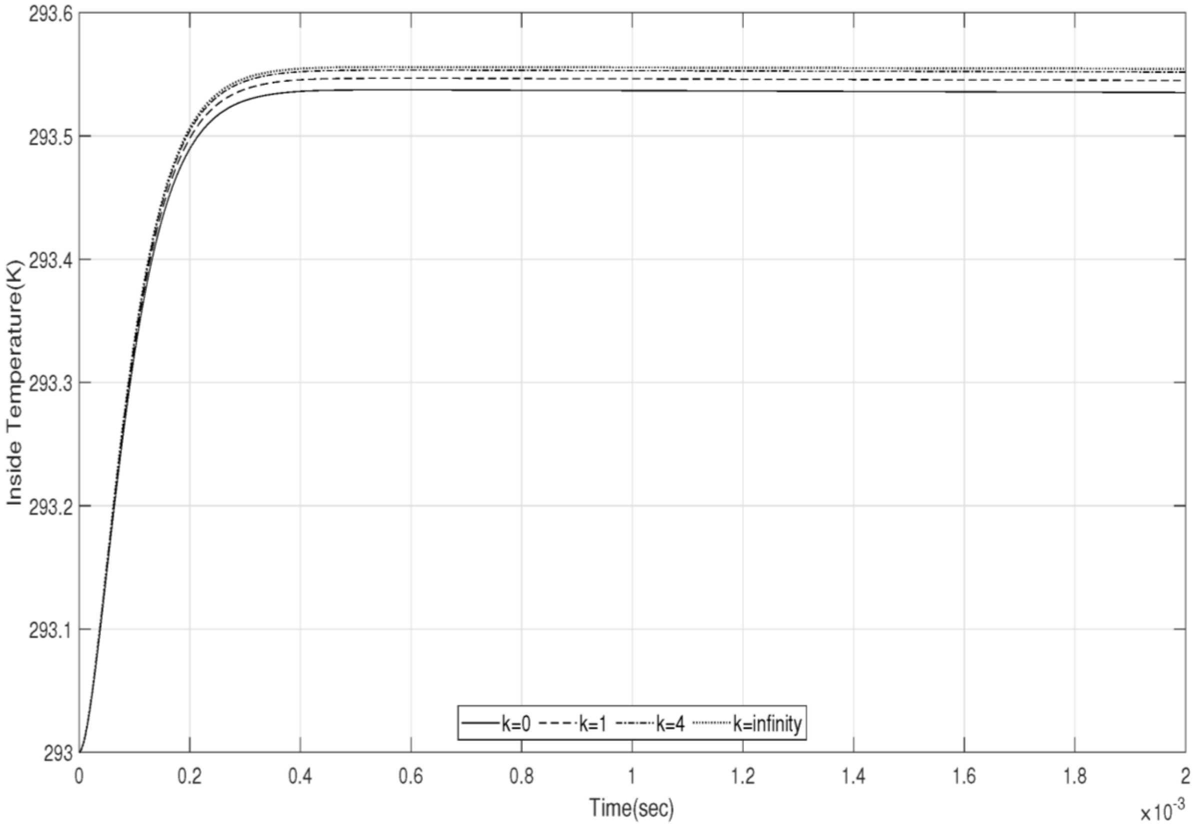

Figure 18 Inside temperature of the shell at $x = 225\ mm$ versus time for different power law indices, case (2).

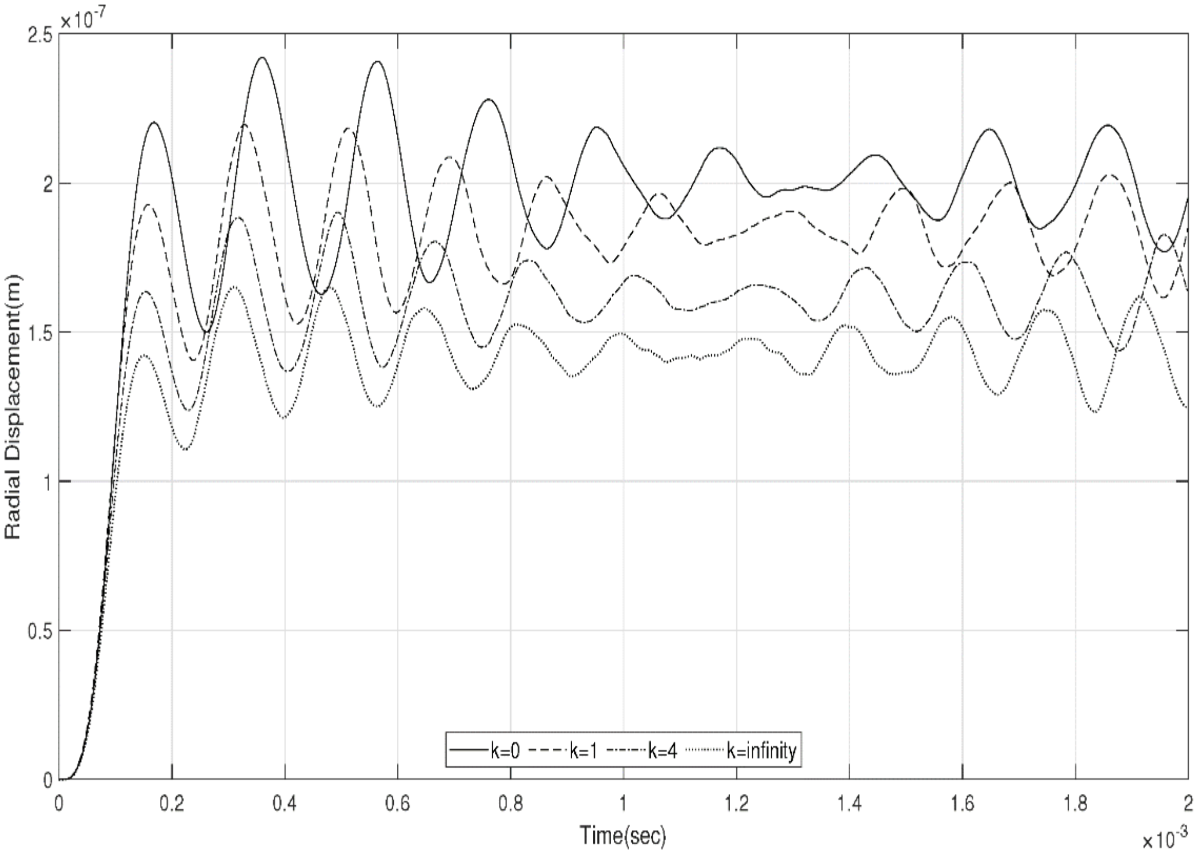

Figure 19 Radial displacement of the shell at $x = 225\ mm$ versus time for different power law indices, case (2).

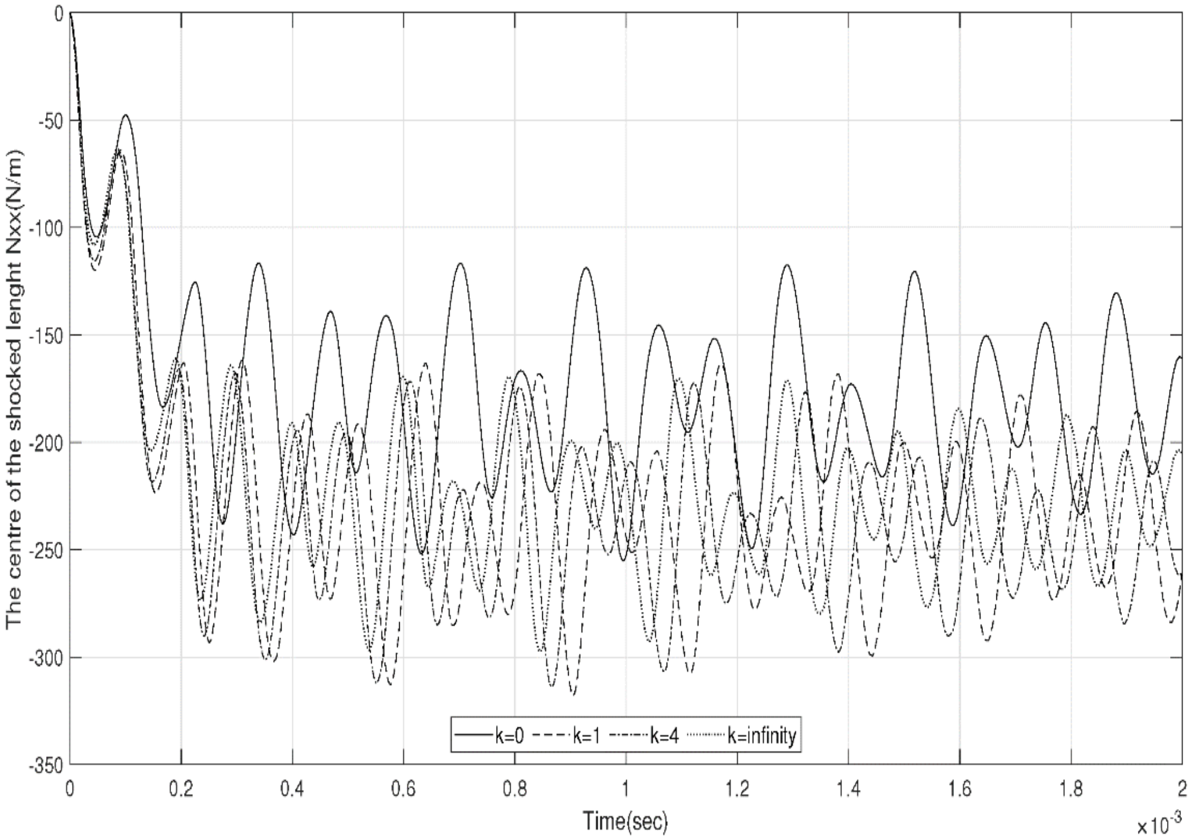

Figure 20 Axial force resultant of the shell at $x = 225\ mm$ versus time for different power law indices, case (2).

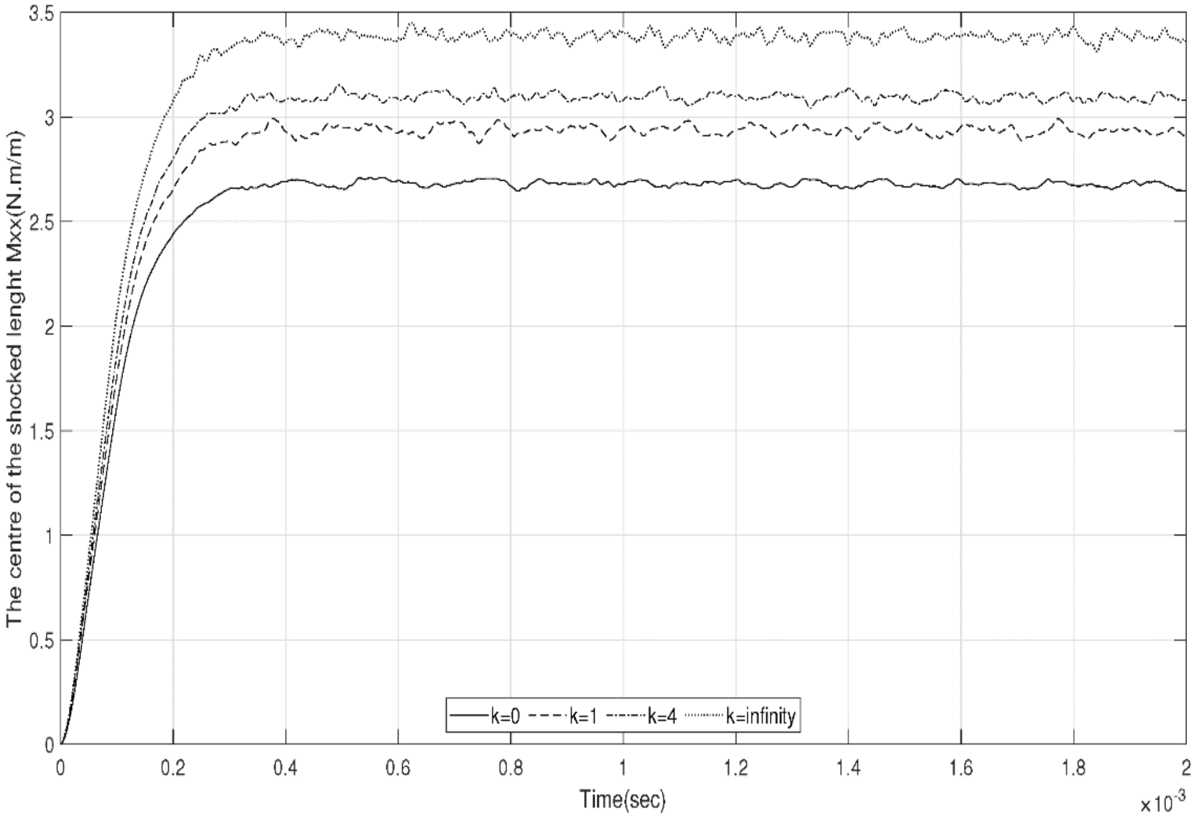

Figure 21 Axial moment resultant of the shell at $x = 225\ mm$ versus time for different power law indices, case (2).

4 Conclusion

In this study, we investigated cylindrical shells composed of functionally graded materials subjected to local symmetric thermal shock. Initially, we derived the equations of motion and energy for cylindrical coordinates using second-order shell theory, followed by their numerical solution. The cylindrical shell we studied belongs to the isotropic FGM category, featuring two phases of metal and ceramic distributed along its thickness. Additionally, we formulated the mechanical and thermal properties of the shell as power-law functions varying across the thickness. Subsequently, we simultaneously solved the motion and energy equations based on coupled thermoelasticity using the Galerkin finite element method in the spatial domain. The cylindrical shell was discretized into quadratic elements along its length, and we solved the problem in the temporal domain using Newmark's numerical method.

We investigated the problem for two thermal shock load rates and employed simply supported boundary conditions. Our analysis enabled us to determine temperature profiles, radial displacements, axial forces, and axial moments along the shell's length. We also generated graphical representations of temperature changes, radial displacements, axial forces, and axial moments over time. Our examination of lateral vibrations across different power-law indices and coupling coefficients, as illustrated in Figures (18) and (22), revealed that vibration frequencies increase while amplitudes decrease with higher power-law indices. Moreover, an increase in the coupling coefficient was found to enhance damping behavior. A noteworthy result from this research is the significance of coupled elasticity theory, particularly when dealing with shells approaching frequency responses.

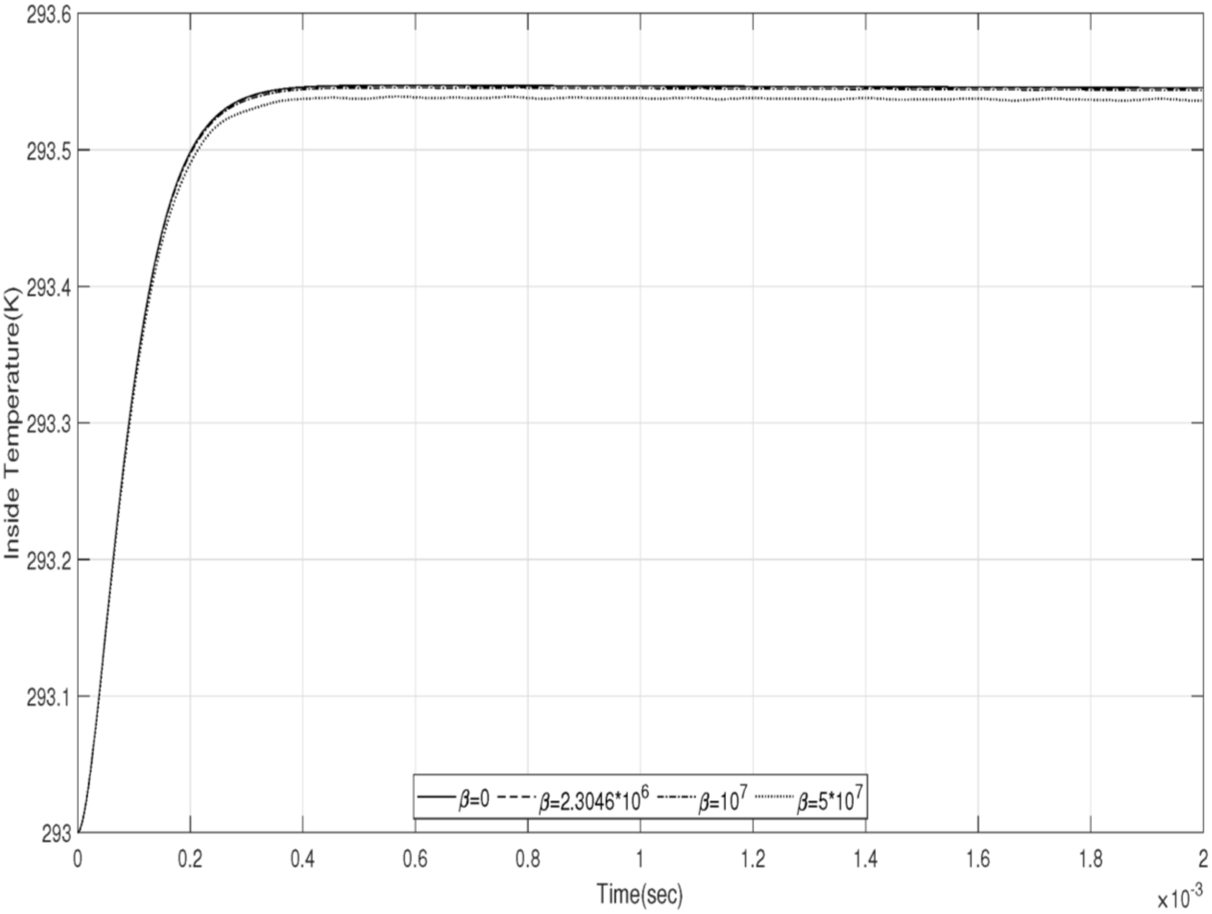

Figure 22 Inside temperature of the shell at $x = 225\ mm$ versus time for different mechanical coupling coefficient, $k = 1$, case (2).

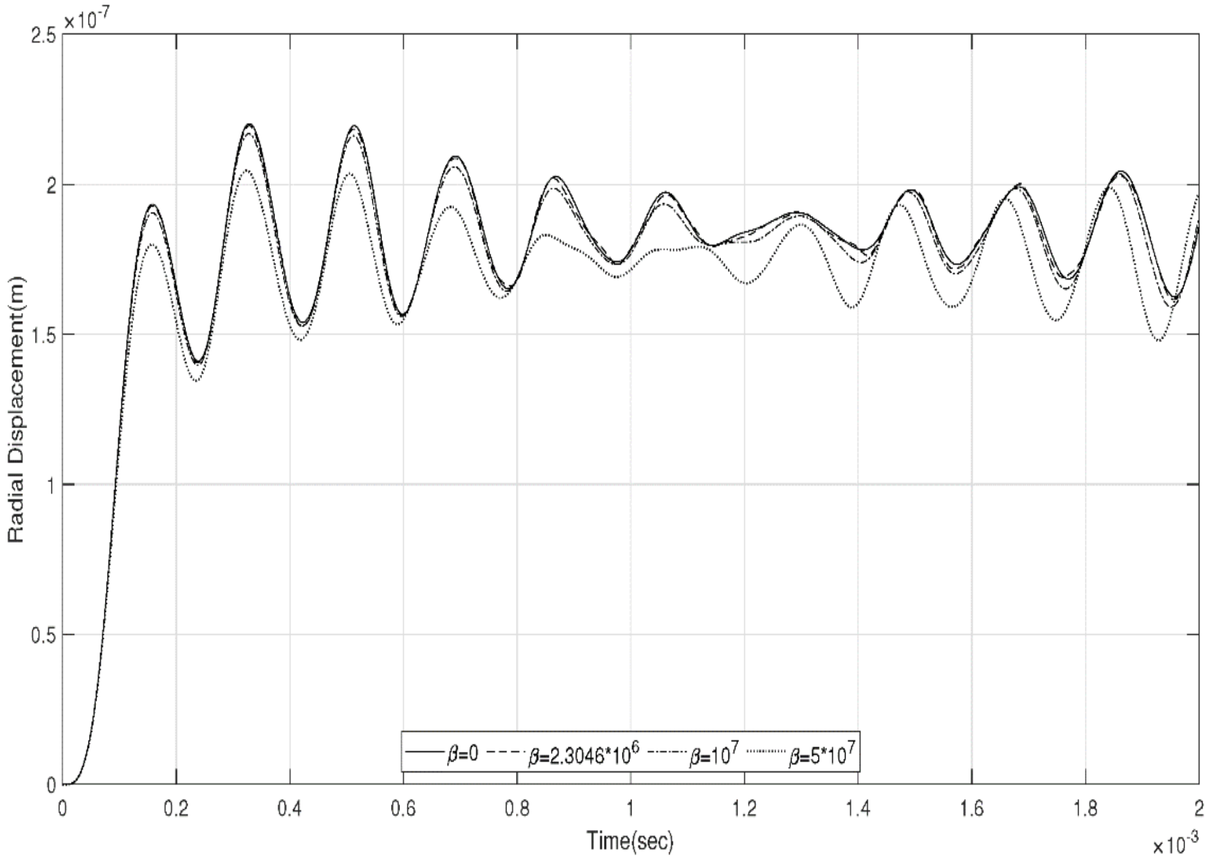

Figure 23 Radial displacement of the shell at $x = 225\ mm$ versus time for different mechanical coupling coefficient, $k = 1$, case (2).

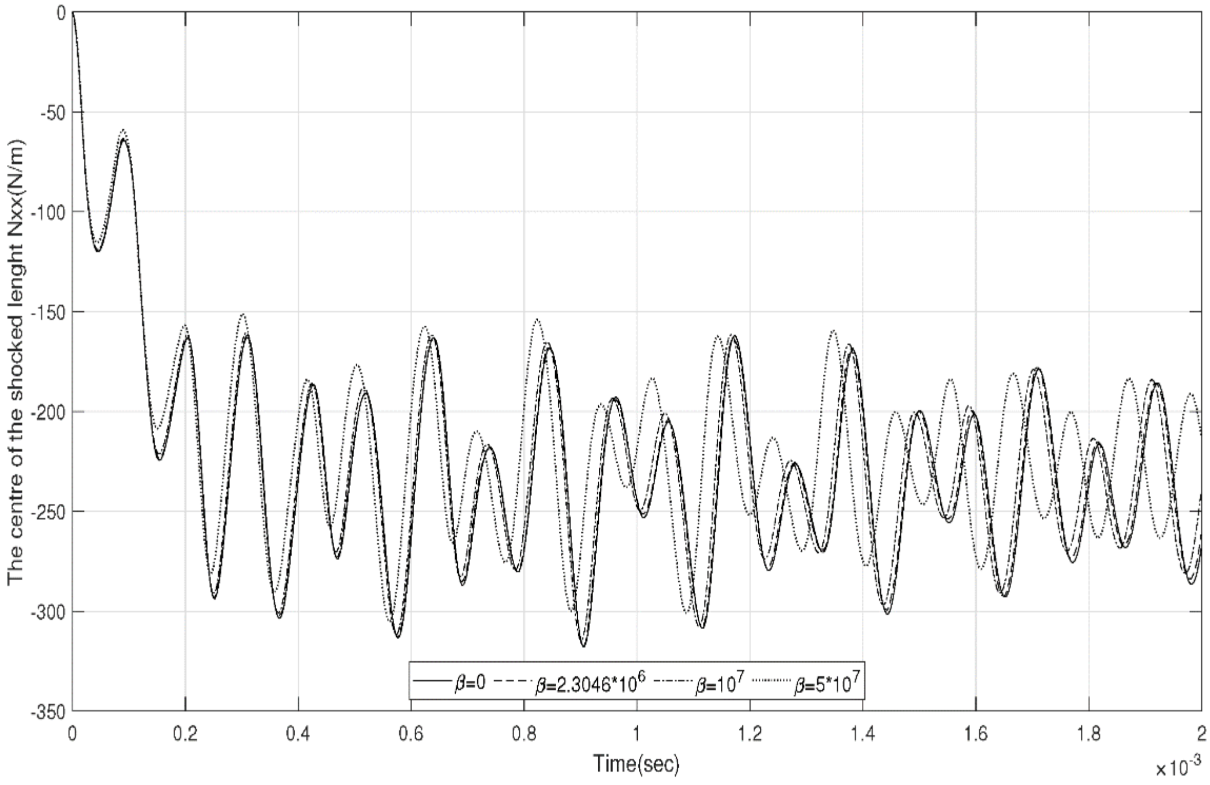

Figure 24 Axial force resultant of the shell at $x = 225\ mm$ versus time for different mechanical coupling coefficient, $k = 1$, case (2).

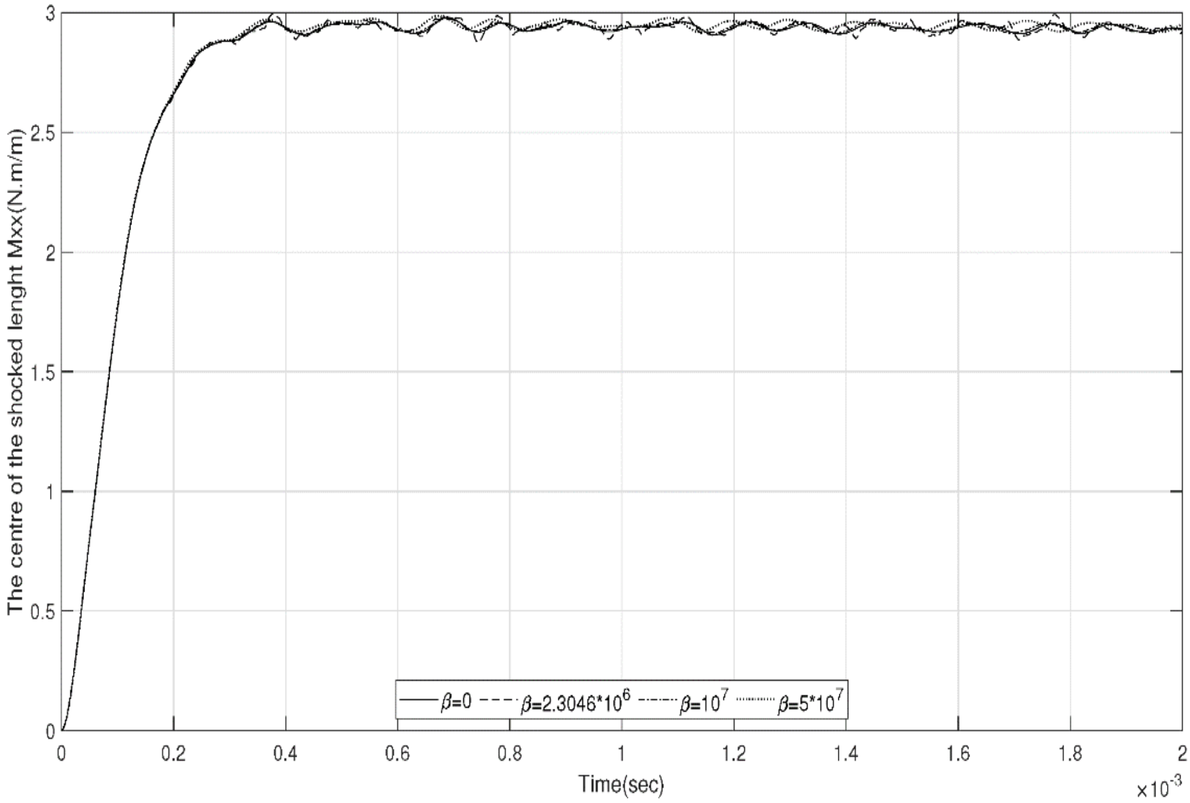

Figure 25 Axial moment resultant of the shell at $x = 225\ mm$ versus time for different mechanical coupling coefficient, $k = 1$, case (2).

References

[1] R. B. Hetnarski, M. R. Eslami, and G. M. L. Gladwell, "*Thermal Stresses: Advanced Theory and Applications*", Second Edition, Berlin: Springer, Vol. 41, pp. 227-231, 2019, https://doi.org/10.1007/978-3-030-10436-8.

[2] E. J. McQuillen, and M. A. Brull, "Dynamic Thermoelastic Response of Cylindrical Shells", *Journal of Applied Mechanics*, Vol. 37, No. 3, pp. 661-670, 1970, https://doi.org/10.1115/1.3408595.

[3] M. R. Eslami, M. Shakeri, and R. Sedaghati, "Coupled Thermoelasticity of an Axially Symmetric Cylindrical Shell", *Journal of Thermal Stresses*, Vol. 17, No. 1, pp. 115-135, 1994, https://doi.org/10.1080/01495739408946250.

[4] H. H. Sherief, and F. A. Hamza, "Generalized Thermoelastic Problem of a Thick Plate under Axisymmetric Temperature Distribution", *Journal of Thermal Stresses*, Vol. 17, No. 3, pp. 435-452, 1994, https://doi.org/10.1080/01495739.2016.1215737.

[5] J. N. Reddy, and C. D. Chin, "Thermomechanical Analysis of Functionally Graded Cylinders and Plates", *Journal of Thermal Stresses*, Vol. 21, No. 6, pp. 593-626, 1998, https://doi.org/10.1080/01495739808956165.

[6] M. R. Eslami, M. Shakeri, A. R. Ohadi, and B. Shiari, "Coupled Thermoelasticity of Shells of Revolution: Effect of Normal Stress and Coupling", *AIAA Journal*, Vol. 37, No. 4, pp. 496-504, 1999, https://doi.org/10.2514/3.14197.

[7] B. Shiari, M. R. Eslami, and M. Shaker, "Thermomechanical Shocks in Composite Cylindrical Shells: A Coupled Thermoelastic Finite Element Analysis", *Scientia Iranica*, Tehran, Iran, 2003, https://www.sid.ir/EN/VEWSSID/J_pdf/95520030105.pdf.

[8] A. Bagri, and M. R. Eslami, "Generalized Coupled Thermoelasticity of Disks Based on the Lord–Shulman Model", *Journal of Thermal Stresses*, Vol. 27, No. 8, pp. 691-704, 2004, https://doi.org/10.1080/01495730490440127.

[9] M. Bakhshi, A. Bagri, and M. R. Eslami, "Coupled Thermoelasticity of Functionally Graded Disk", *Mechanics of Advanced Materials and Structures*, Vol. 13, No. 3, pp. 219-225, 2006, https://doi.org/10.1080/15376490600582719.

[10] A. Bahtui, and M. R. Eslami, "Generalized Coupled Thermoelasticity of Functionally Graded Cylindrical Shells", *International Journal*, 2007, https://doi.org/10.1002/nme.1782.

[11] M. H. Babaei, M. Abbasi, and M. R. Eslami, "Coupled Thermoelasticity of Functionally Graded Beams", *Journal of Thermal Stresses*, Vol. 31, No. 8, pp. 680-697, 2008, https://doi.org/10.1080/01495730802193930.

[12] A. Bagri, and M. R. Eslami, "Generalized Coupled Thermoelasticity of Functionally Graded Annular Disk Considering the Lord–Shulman Theory", *Composite Structures*, Vol. 83, No. 2, pp .168-179, 2008, https://doi.org/10.1016/j.compstruct.2007.04.024.

[13] S. M. Hosseini, "Coupled Thermoelasticity and Second Sound in Finite Length Functionally Graded Thick Hollow Cylinders (without Energy Dissipation)", *Materials and Design*, Vol. 30, No. 6, pp. 2011-2023, 2009, https://doi.org/10.1016/j.matdes.2008.08.048.

[14] Y. Heydarpour, and M. M. Aghdam, "Transient Analysis of Rotating Functionally Graded Truncated Conical Shells Based on the Lord-Shulman Model", *Thin-Walled Structures*, Vol. 104, pp. 168-184, 2016, doi: https://doi.org/10.1016/j.tws.2016.03.016.

[15] M. R. Jafarinezhad, and M. R. Eslami, "Coupled Thermoelasticity of FGM Annular Plate under Lateral Thermal Shock", *Composite Structures*, Vol. 168, pp. 758-771, 2017, https://doi.org/10.1016/j.compstruct.2017.02.071.

[16] H. R. Esmaeili, H. Arvin, and Y. Kiani, "Axisymmetric Nonlinear Rapid Heating of FGM Cylindrical Shells", *Journal of Thermal Stresses*, Vol. 42, No. 4, pp. 490-505, 2019, https://doi.org/10.1080/01495739.2018.1498756.

[17] P. K. Zeverdejani, and Y. Kiani, "Radially Symmetric Response of an FGM Spherical Pressure Vessel under Thermal Shock using the Thermally Nonlinear Lord-Shulman Model", *International Journal of Pressure Vessels and Piping*, Vol. 182, pp. 104-065, 2020, https://doi.org/10.1016/j.ijpvp.2020.104065.

[18] M. Sakha, and M. R. Eslami, "Generalized Thermoelasticity of Beams under Partial Thermal Shock", *Applied Mathematical Modelling*, Vol. 79, pp. 402-413, 2020, https://doi.org/10.1016/j.apm.2019.10.043.

[19] M. R. Eslami, "*Finite Elements Methods in Mechanics*", Switzerland: Springer International Publishing, Switzerland, 2014, https://doi.org/10.1007/978-3-319-08037-6_17.

[20] A. Bahtui, and M. R. Eslami, "Coupled Thermoelasticity of Functionally Graded Cylindrical Shells", *Mechanics Research Communications*, Vol. 34, No. 1, pp. 1-18, 2007, https://doi.org/10.1016/j.mechrescom.2005.09.003.

[21] T. Yang, W. L. Li, and L. Dai, "Vibrations of Cylindrical Shells", *Advances in Vibration Engineering and Structural Dynamics*, 2012, http://dx.doi.org/10.5772/51816.

Appendix

$$A_{1,2,3,4,5,6} = \int_z \frac{E(z)}{1-\nu^2}\left(\frac{\nu}{R}, z\frac{\nu}{R}, \frac{1}{z+R}, \left(1+\frac{z}{R}\right), z\left(1+\frac{z}{R}\right), z^2\left(1+\frac{z}{R}\right)\right) dz$$

$$\acute{A}_1 = \int_z \frac{E(z)}{2(1+\nu)}\left(1+\frac{z}{R}\right) dz$$

$$B_{1,2,3,4,5} = \int_z \frac{E(z)\alpha(z)}{1-\nu}\left(\frac{1}{R}, \frac{z}{R}, z^2, \left(1+\frac{z}{R}\right), z\left(1+\frac{z}{R}\right), z^2\left(1+\frac{z}{R}\right)\right) dz \tag{1}$$

$$\acute{B}_{1,2,3,4,5} = \int_z \frac{E(z)\alpha(z)}{1-2\nu}\left(1, z, z^2, \frac{1}{z+R}, \frac{z}{z+R}\right) dz$$

$$D_{1,2,3,4,5} = \int_z K(z)\left(1, z, z^2, \frac{1}{z+R}, \frac{z}{z+R}\right) dz$$

$$F_{1,2,3} = \int_z \rho(z)\,(1, z, z^2) dz$$